Geochemistry Geophysics Geosystems G3
AN ELECTRONIC JOURNAL OF THE EARTH SCIENCES
Published by AGU and the Geochemical Society

Article
Volume 5, Number 6
19 June 2004
Q06004, doi:10.1029/2003GC000683
ISSN: 1525-2027

Impact of atmospheric CO_2 and galactic cosmic radiation on Phanerozoic climate change and the marine $\delta^{18}O$ record

K. Wallmann
GEOMAR Research Center, Wischhofstrasse 1–3, 24148 Kiel, Germany (kwallmann@geomar.de)

[1] A new model is developed and applied to simulate the Phanerozoic evolution of seawater composition (dissolved Ca, Sr, dissolved inorganic carbon, alkalinity, pH, $\delta^{18}O$), marine carbonates (Sr/Ca, $^{87}Sr/^{86}Sr$, $\delta^{13}C$, $\delta^{18}O$), atmospheric CO_2 and surface temperature. The marine carbonate records (Sr/Ca, $^{87}Sr/^{86}Sr$, $\delta^{13}C$) are used to reconstruct changes in volcanic/tectonic activity and organic carbon burial over the Phanerozoic. Seawater pH is calculated assuming saturation with respect to calcite and considering the changing concentration of dissolved Ca documented by brine inclusion data. The depth of calcite saturation is allowed to vary through time and the effects of changing temperature and pressure on the stability constants of the carbonate system are considered. Surface temperatures are calculated using the GEOCARB III approach considering also the changing flux of galactic cosmic radiation (GCR). It is assumed that GCR cools the surface of the Earth via enhanced cloud formation at low altitudes. The $\delta^{18}O$ of marine carbonates is calculated considering the changing isotopic composition of seawater, the prevailing surface temperatures and seawater pH. Repeated model runs showed that the trends observed in the marine $\delta^{18}O$ record can only be reproduced by the model if GCR is allowed to have a strong effect on surface temperature. The climate evolution predicted by the model is consistent with the geological record. Warm periods (Cambrian, Devonian, Triassic, Cretaceous) are characterized by low GCR levels. Cold periods during the late Carboniferous to early Permian and the late Cenozoic are marked by high GCR fluxes and low pCO_2 values. The major glaciations occurring during these periods are the result of carbon cycling processes causing a draw-down of atmospheric CO_2 and a coevally prevailing dense cloud cover at low-altitudes induced by strong GCR fluxes. The two moderately cool periods during the Ordovician - Silurian and Jurassic - early Cretaceous are characterized by both high pCO_2 and GCR levels so that greenhouse warming compensated for the cooling effect of low-altitude clouds. The very high Jurassic $\delta^{18}O$ values observed in the geological record are caused by low pH values in surface waters rather than cold surface conditions.

Components: 14,117 words, 13 figures, 5 tables.

Keywords: box modeling; galactic cosmic radiation; geochemical evolution; marine $d^{18}O$ record; Phanerozoic climate change; seawater pH.

Index Terms: 1010 Geochemistry: Chemical evolution; 1620 Global Change: Climate dynamics (3309); 2479 Ionosphere: Solar radiation and cosmic ray effects.

Received 22 December 2003; **Revised** 5 March 2004; **Accepted** 26 March 2004; **Published** 19 June 2004.

Wallmann, K. (2004), Impact of atmospheric CO_2 and galactic cosmic radiation on Phanerozoic climate change and the marine $\delta^{18}O$ record, *Geochem. Geophys. Geosyst.*, *5*, Q06004, doi:10.1029/2003GC000683.

Copyright 2004 by the American Geophysical Union

1. Introduction

[2] Proxy data [*Royer et al.*, 2001] and box modeling [*Berner and Kothavala*, 2001] demonstrate that the atmospheric partial pressure of CO_2 (pCO_2) has oscillated over the Phanerozoic due to changing rates of mantle degassing, weathering, organic carbon burial and carbonate turnover [*Berner*, 1991b; *Berner*, 1994; *Berner and Kothavala*, 2001; *Hansen and Wallmann*, 2003; *Wallmann*, 2001a]. The simulated changes in pCO_2 correspond roughly to paleoclimatic reconstructions [*Crowley and Berner*, 2001] supporting the view that Phanerozoic climate change has been driven mainly by changes in atmospheric pCO_2. A different picture emerges from the evaluation of $\delta^{18}O$ values in marine carbonate fossils [*Veizer et al.*, 1997, 1999, 2000]. These data show regular oscillations with a shorter period indicating changes in surface temperatures at low latitudes that are consistent with some paleoclimatic reconstructions [*Frakes et al.*, 1992; *Boucot and Gray*, 2001] but not with surface temperatures derived from pCO_2 modeling [*Crowley and Berner*, 2001; *Veizer et al.*, 2000]. This difference may be regarded as evidence for the decoupling of pCO_2 and climate evolution [*Veizer et al.*, 2000]. The latter view is supported by recent modeling of galactic cosmic radiation (GCR) over the last billion years [*Shaviv*, 2002a]. These new data show a surprisingly strong correlation with $\delta^{18}O$-based temperature reconstructions [*Shaviv and Veizer*, 2003] suggesting that climate change has been driven mainly by cosmic radiation. Nevertheless, temperatures calculated from the marine $\delta^{18}O$ record are met with skepticism because the extremely low Jurassic surface temperatures derived from this proxy are not consistent with other observations [*Crowley and Berner*, 2001].

[3] GCR fluxes are believed to affect climate change on short timescales, as well, because the intensity of galactic radiation reaching the Earth is strongly modulated by rapid changes in the sun's activity. The effect of solar activity on GCR fluxes has been clearly documented through the strong correlation observed between the temporal variability of GCR - measured at the Earth surface in ionization chambers since 1934 - and the sunspot number [*Marsh and Svensmark*, 2000a]. GCR is the dominant source of atmospheric ionization at altitudes of 0–35 km and in the troposphere ionization may contribute to the formation of cloud condensation nuclei [*Marsh and Svensmark*, 2000b]. Thus it seems to be possible that the cloud properties may be altered by GCR. Satellite observations revealed indeed a correlation between global cloud cover and GCR flux over the last two decades of the 20th century [*Svensmark*, 1998; *Svensmark and Friis-Christensen*, 1997]. The correlation is especially strong for clouds at low altitudes (<3 km) whereas cloud formation at higher altitudes is not well correlated with GCR fluxes [*Marsh and Svensmark*, 2000b]. Clouds affect the global climate in various ways. The net radiative impact of a particular cloud is mainly dependent upon its height above the surface and its optical thickness. Low and optically thick clouds tend to cool and it is this kind of cloudiness which is well correlated with GCR fluxes [*Marsh and Svensmark*, 2000b]. Thus its seems to be possible that global surface temperatures are reduced during periods of enhanced GCR. Average northern hemisphere temperatures show indeed a good correlation with inverted GCR fluxes over the period of 1935 till 1985 confirming the postulated GCR-climate link [*Svensmark*, 1998]. Holocene climate change seems to be affected by GCR on centennial and millennial scales, as well, because the production rate of cosmogenic isotopes (^{14}C, ^{10}Be) shows a very good correlation with proxy data from various climate archives [*Bond et al.*, 2001; *Neff et al.*, 2001; *Hu et al.*, 2003; *Niggemann et al.*, 2003]. The observed climate effects may be due to GCR-induced cloud formation or could be caused by changes in solar luminosity [*Bond et al.*, 2001]. The role of GCR in cloud formation is not fully understood and coeval changes in total solar irradiance are too small to affect surface temperatures significantly [*Foukal*, 2002]. Hence the physical mechanisms causing the well-documented correlation between solar activity and climate remain enigmatic and have to be resolved in future studies.

[4] The pH of seawater plays an important role in the controversial debate on paleoclimate. It is

strongly affected by changes in pCO_2 and it has a significant impact on the $\delta^{18}O$ values of marine carbonates [*Spero et al.*, 1997; *Usdowski and Hoefs*, 1993; *Zeebe and Wolf-Gladrow*, 2001; *Zeebe*, 1999, 2001] which has not been considered in the calculation of $\delta^{18}O$-based temperatures. Moreover, the pH of seawater depends on the concentrations of dissolved inorganic carbon and carbonate alkalinity which are in turn affected by the concentration of dissolved calcium ions and the saturation state of the ocean with respect to calcite. Thus secular trends of seawater pH also mirror changes in bulk ocean chemistry through time.

[5] In the following, I present a new box model of the global carbon cycle and Phanerozoic climate evolution which considers the impact of GCR on surface temperature and pCO_2. New Phanerozoic records of temperature, seawater pH, and pCO_2 change are produced which show very high pCO_2 values but moderate surface temperatures for the Jurassic and Ordovician. It is demonstrated that enhanced pCO_2 compensates for the cooling via enhanced GCR fluxes during these periods. The marine $\delta^{18}O$ record is shown to reflect both changes in surface temperature and seawater pH. The low pH of Jurassic seawater is responsible for the high $\delta^{18}O$ values observed in carbonate fossils which have been previously mistaken as indication for severe cooling.

2. Set-Up of the Box Model

[6] The box model has been designed combining elements of the GEOCARB III model [*Berner and Kothavala*, 2001] with other flux parameterizations defining the turnover of water [*Wallmann*, 2001b] carbon and Sr [*Hansen and Wallmann*, 2003; *Wallmann*, 2001a].

2.1. Carbon and Sr Cycling

[7] The model considers mantle degassing, continental weathering, alteration of oceanic crust, turnover of organic carbon, and recycling of carbon at subduction zones. In the following, I briefly present the major changes of the model with respect to previous approaches [*Berner and Kothavala*, 2001; *Hansen and Wallmann*, 2003; *Wallmann*, 2001a]. Complete lists of all fluxes, parameter values, and reservoirs are given in the Appendix (Tables A1–A5).

[8] Rates of volcanic and tectonic activity (f_{VO}) are no longer reconstructed from eustatic sea level changes [*Berner and Kothavala*, 2001] but from the marine $^{87}Sr/^{86}Sr$ record [*Veizer et al.*, 1999]. Global sea level is affected by many different factors, such as the formation of large continental ice shields, seafloor spreading rates and the emplacement of oceanic flood basalts, mountain-building and sedimentation, making sea level change a rather poor proxy for changes in spreading and volcanic activity. On the other hand, the $^{87}Sr/^{86}Sr$ ratio in seawater clearly reflects the input of isotopically depleted Sr from hydrothermal systems at spreading centers and the weathering of young volcanic deposits (Figure 1a). The rates of tectonic and volcanic activity (f_{VO}) are thus calculated as:

$$f_{VO} = k_V \cdot \left(\left({}^{87}Sr/_{86}SR \right)_{MOD} - \left({}^{87}Sr/_{86}SR \right)_{DAT} \right) \qquad (1)$$

where $(^{87}Sr/^{86}Sr)_{MOD}$ and $(^{87}Sr/^{86}Sr)_{DAT}$ are the isotope ratios in seawater calculated in the model and recorded in marine carbonates [*Veizer et al.*, 1999], respectively, and k_V is a kinetic constant. With this parameterization the f_{VO} variable is dynamically adjusted so that the calculated isotopic ratio is always close to the secular trend documented in the marine carbonate record. The kinetic constant is set to a large value (10^5) guaranteeing a very small deviation (< 1%) between measured and modeled isotope ratios for all model runs.

[9] Recently improved estimates of the CO_2 contents in the upper mantle indicate rather low rates of CO_2 degassing at mid-ocean ridge spreading centers ($0.9 \pm 0.3 \times 10^{+18}$ mol Myr^{-1} [*Saal et al.*, 2002]). Thus the total rate of mantle-CO_2 degassing at spreading centers, subduction zones, and intraplate volcanoes was reduced to $1.5 \times 10^{+18}$ mol Myr^{-1}.

[10] Dissolved Sr concentrations and $^{87}Sr/^{86}Sr$ ratios in seawater are calculated considering the inputs of Sr and ^{87}Sr into the ocean from carbonate and silicate weathering and the corresponding

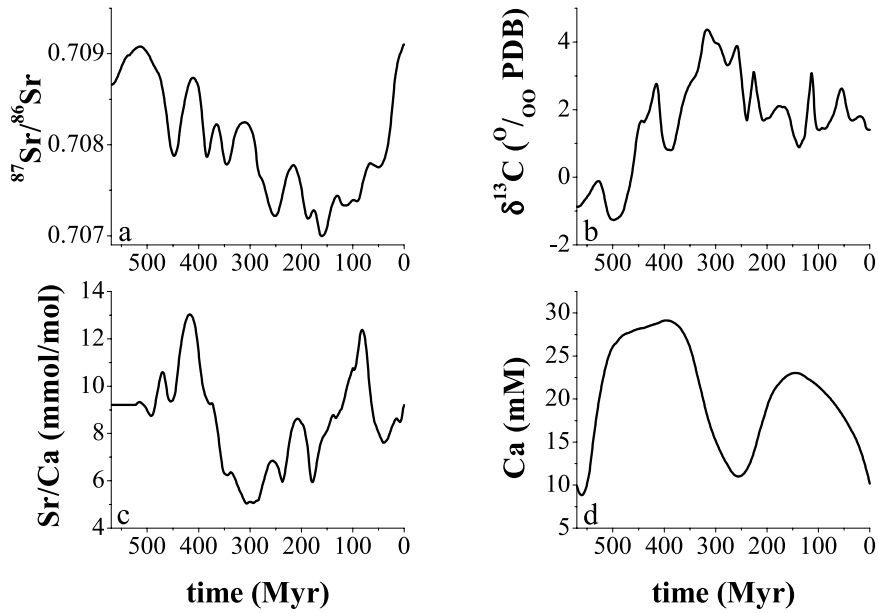

Figure 1. Secular trends in the isotopic and chemical composition of seawater used as forcing to the model. (a) Change in the $^{87}Sr/^{86}Sr$ ratio of seawater as recorded in marine carbonates [*Veizer et al.*, 1999]. (b) Change in the $\delta^{13}C$ value of inorganic carbon dissolved in seawater as recorded in marine carbonates [*Veizer et al.*, 1999]. (c) Change in the Sr/Ca ratio of seawater derived from marine carbonate data [*Lear et al.*, 2000; *Steuber and Veizer*, 2002]. (d) Change in the dissolved Ca concentration derived from brine inclusions in evaporite minerals [*Horita et al.*, 2002]. $^{87}Sr/^{86}Sr$, $\delta^{13}C$, and Sr/Ca data were binned into 10–20 Myr intervals and averaged using a 30–60 Myr moving average. In all simulations, the $^{87}Sr/^{86}Sr$, $\delta^{13}C$, and Sr/Ca values calculated in the model are forced to follow the prescribed values shown in Figures 1a–1c within a tolerance of 1% using equations (1), (2), and (4). Ca concentrations are not calculated in the model but are taken directly from the proxy record (Figure 1d).

hydrothermal fluxes (Table A1). A new and better estimate for the modern hydrothermal Sr flux ($3.1 \pm 0.8 \times 10^{15}$ mol Sr Myr^{-1} [*Davis et al.*, 2003]) is applied in the modeling. The removal flux of Sr from the ocean is calculated as:

$$F_B^{Sr} = k_{BSr} \cdot \left({}^{Sr_{MOD}}/_{Ca_{DAT}} - \left({}^{Sr}/_{Ca} \right)_{DAT} \right) \quad (2)$$

where Sr_{MOD}, Ca_{DAT}, and $(Sr/Ca)_{DAT}$ are concentrations and concentration ratios in seawater calculated in the model (MOD) and recorded in marine carbonates and brine inclusions (DAT) and k_{BSr} is a kinetic constant. F_B^{Sr} gives the removal of Sr from seawater via carbonate accumulation, alteration of oceanic crust, inverse weathering, and other processes such as the alteration of sedimentary volcanic ashes. The magnitude of important Sr removal fluxes is virtually unknown both for modern and ancient oceans. Thus the rather well documented changes in seawater Sr/Ca ratios [*Lear et al.*, 2003; *Steuber and Veizer*, 2002] are used to constrain the overall removal flux (Figure 1c). Seawater Ca concentrations used in the calculation of Sr/Ca ratios are not determined in the model but are taken from a recent reconstruction [*Horita et al.*, 2002] based on brine inclusion data (Figure 1d).

[11] The rates of physical erosion (f_{ER}) are redefined using Ronov's data on the accumulation rate of terrigenous deposits over the Phanerozoic [*Ronov*, 1993] as listed in *Berner and Kothavala* [2001]. The original deposition rates prior to post-depositional erosion and metamorphism of sedimentary rocks are calculated from Ronov's data applying a first order decay constant of 3×10^{-3} Myr^{-1} [*Gregor*, 1985; *Tardy et al.*, 1989]. Subsequently, they are normalized to the Quaternary value to obtain the nondimensional f_{ER} variable (Figure 2a). Erosion rates are considered in the calculation of carbonate weathering because recent weathering studies demonstrate that mountain-building and physical erosion have a very

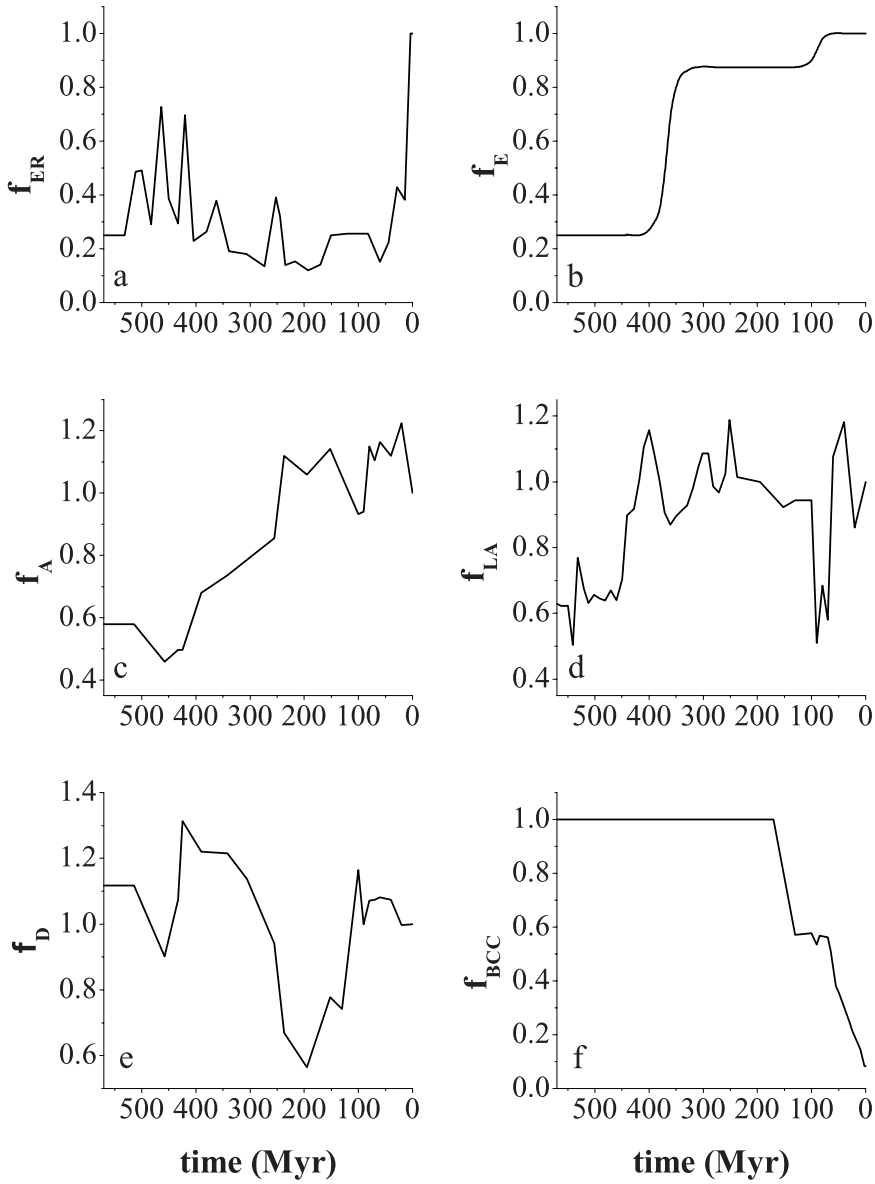

Figure 2. Nondimensional functions used as forcing to the model. (a) Change in physical erosion rate calculated from accumulation rates of terrigenous sediments [*Berner and Kothavala*, 2001; *Ronov*, 1993] applying a decay constant of 3×10^{-3} Myr^{-1} [*Gregor*, 1985]. (b) Change in the efficiency of chemical weathering due to the spread of land plants and angiosperms [*Berner and Kothavala*, 2001]. (c) Change in land area exposed to weathering and precipitation [*Gibbs et al.*, 1999; *Otto-Bliesner*, 1995]. (d) Change in carbonate rock area exposed to weathering [*Bluth and Kump*, 1991; *Gibbs et al.*, 1999]. (e) Change in runoff due to paleogeographic evolution and changing continentality [*Gibbs et al.*, 1999; *Otto-Bliesner*, 1995]. (f) Change in the fraction of sedimentary carbonate accumulating on continental crust rather than oceanic crust [*Hay*, 1998]. All rates are normalized to their Quaternary values to obtain nondimensional functions [*Berner et al.*, 1983].

strong effect not only on silicate but also on carbonate weathering rates [*Jacobson et al.*, 2002, 2003]. The other nondimensional variables applied in the model are shown in Figures 2b–2f. They are mainly taken from the GEOCARB III model considering new estimates of ice-free land area and continental runoff over the last 250 Myr [*Gibbs et al.*, 1999].

[12] Uptake of dissolved inorganic carbon during alteration of oceanic crust (F_{ALT}) is taken to be

inversely proportional to the amount of pelagic carbonate sediments deposited on oceanic crust (CO):

$$F_{ALT} = \frac{CO(Q)}{CO} \cdot (r_{ALT} \cdot (f_{VO} - 1) + 1) \cdot F_{ALT}(Q) \quad (3)$$

where CO(Q) and $F_{ALT}(Q)$ are the corresponding Quaternary values, r_{ALT} is the fraction of authigenic $CaCO_3$ formation occurring close to spreading centers [*Wallmann*, 2001a], and f_{VO} is the rate of volcanic/tectonic activity derived from $^{87}Sr/^{86}Sr$ modeling. The rationale for this parameterization lies in the observation that the modern rates of low-temperature ridge flank circulation and authigenic $CaCO_3$ precipitation are limited by the development of a thick sedimentary cover [*Fisher and Becker*, 2000] composed mainly of pelagic carbonates [*Archer*, 1996].

[13] The burial rate of particulate organic carbon (F_{BO}) in sediments is calculated from the marine $\delta^{13}C$ record (Figure 1b):

$$F_{BO} = k_{BO} \cdot (\delta^{13}C_{DAT} - \delta^{13}C_{MOD}) \quad (4)$$

where k_{BO} is a kinetic constant, $\delta^{13}C_{DAT}$ is the $\delta^{13}C$ value of dissolved inorganic carbon in seawater derived from marine carbonate data [*Veizer et al.*, 1999] and $\delta^{13}C_{MOD}$ is the corresponding value calculated in the model. The marine $\delta^{13}C$ values were calculated as outlined in *Wallmann* [2001a] considering all major carbon fluxes and the changing isotopic fractionation (α_{POC}) between marine particulate organic carbon (POC) and marine carbonates [*Hayes et al.*, 1999]. The isotopic composition of CO_2 released via POC weathering is allowed to change through time following the secular evolution of $\delta^{13}C$ values of marine POC [*Hayes et al.*, 1999].

2.2. Calculation of Surface Temperatures

[14] The average global surface temperature T_S is calculated using an enhanced GEOCARB III formulation which takes into account the effect of cosmic radiation (Figure 3):

$$T_S = \Gamma \cdot \ln RCO_2 - W_S \cdot \frac{t}{570} + GEOG - \Delta_{COS} \cdot (f_{GCR} - 1) + T(Q) \quad (5)$$

where Γ gives the relation between temperature and RCO_2, RCO_2 is the atmospheric partial pressure of CO_2 normalized to the Quaternary value (230 μatm), W_S defines the impact of increasing solar luminosity on surface temperature [*Berner and Kothavala*, 2001], GEOG describes the effect of paleogeography on albedo and surface temperature [*Berner and Kothavala*, 2001; *Otto-Bliesner*, 1995], Δ_{GCR} gives the effect of the galactic cosmic radiation flux on surface temperature, f_{GCR} is the changing flux of galactic cosmic radiation (Figure 3) [*Shaviv and Veizer*, 2003] and T(Q) is the average Quaternary surface temperature (13.5°C) [*Wallmann*, 2001a]. W_S has a constant value of 7.4°C whereas Γ is high for cold periods and low for warmer periods (Figure 4b) due to the effects of large continental ice shields on albedo and surface temperature [*Kothavala et al.*, 1999, 2000a, 2000b].

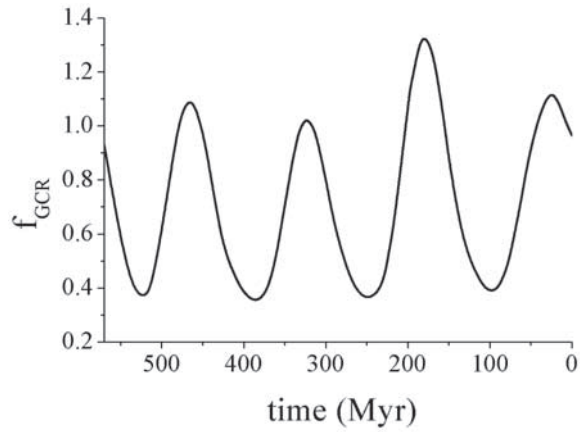

Figure 3. Change in the relative intensity of galactic cosmic radiation received by our solar system over the Phanerozoic [*Shaviv*, 2002a; *Shaviv and Veizer*, 2003].

[15] The intensity of GCR does not only change on long geological timescales but also on much shorter periods because solar activity through the solar wind strongly reduces the GCR flux that reaches the Earth. Therefore the relation between GCR intensity and surface temperature can be derived from field measurements. The Δ_{cos} value used in the standard case is based on data measured at the University of Chicago Neutron Monitor Stations in Hawaii and Peru at altitudes of ~3 km where the relative change in both GCR intensity and low-altitude cloud cover was 6–7% over the period of 1982–1987 [*Shaviv*, 2002b]. Applying a linear relation between cloud cover and GCR and using model-based estimates for the impact

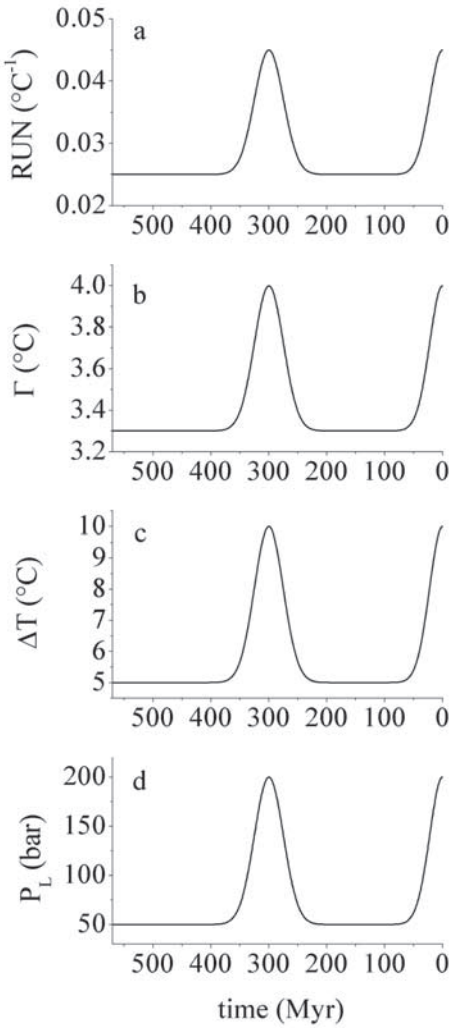

Figure 4. Variations in model parameter values applied to simulate the effects of major glaciations during the late Permian - early Carbonaceous and late Cenozoic. (a) Impact of surface temperature on runoff [*Berner and Kothavala*, 2001]. (b) Relation between pCO_2 and surface temperature [*Berner and Kothavala*, 2001]. (c) Difference between surface temperature and water temperature at the calcite saturation depth. (d) Pressure at the calcite saturation depth.

of cloud cover on surface temperature, *Shaviv* [2002b] postulated that a 1% increase in GCR reduces the surface temperature by about 0.14°C (corresponding to Δ_{cos} = 14°C).

2.3. Calculation of Seawater pH and Carbonate Equilibria

[16] Parameters of the carbonate system are determined using the concentrations of total dissolved inorganic carbon (TC = CO_2 + HCO_3 + CO_3) and carbonate alkalinity (CA = HCO_3 + 2 CO_3) which are calculated in the carbon box model as major time-dependent variables (Table A5). Stability constants defining the carbonate system in seawater are taken from *Zeebe and Wolf-Gladrow* [2001].

[17] In the modern ocean, dissolved CO_2 concentrations increase with water depth due to the degradation of sinking organic particles. The CO_2 increase and the rising pressure induce a change in the carbonate chemistry of deeper water masses favoring the dissolution of calcite. The deep water is thus undersaturated while the upper water masses are oversaturated with respect to calcite. At a certain depths L seawater is saturated with respect to calcite. In today's ocean the saturation level L is situated at an average water depth of about 2 km [*Archer*, 1996]. In the North Pacific the saturation is reached at a much shallower depth level (≈750 m) than in the North Atlantic (≈4300 m) because the old Pacific intermediate and deep water masses contain abundant CO_2 derived from organic matter degradation [*Millero*, 1996]. The carbonate ion concentration at depth L is calculated from CA and TC using the following equation:

$$CO_3 = \frac{CA(K_1 - 4K_2) - K_1TC + \sqrt{K_1(CA(K_1 - 4K_2)(CA - 2TC) + K_1TC^2)}}{2(K_1 - 4k_2)} \quad (6)$$

where the first and second dissociation constants of carbonic acid (K_1 and K_2) depend on temperature, pressure and salinity [*Zeebe and Wolf-Gladrow*, 2001]. The temperature prevailing at the saturation level (T_L) is related to the surface temperature (T_S) calculated in the model (equation (5)) as:

$$T_L = T_S - \Delta T \quad (7)$$

The temperature difference ΔT is close to 10°C in the modern ocean because deep water masses forming at high latitudes have low temperatures. During greenhouse periods, the temperatures at high latitudes are strongly enhanced so that deep water masses are much warmer and ΔT is reduced to smaller values [*Barron et al.*, 1995]. Therefore

ΔT is treated as a time dependent variable with larger values during major glaciations and small values during greenhouse periods (Figure 4c). Sediment data clearly show that the saturation level was shifted to shallow water depths during the warm Cretaceous [*Van Andel*, 1975]. Thus it is assumed that L and the corresponding pressure show a regular variation over Phanerozoic climate cycles (Figure 4d). The salinity of seawater is assumed to remain at a constant level of 35 throughout the Phanerozoic because brine inclusion data [*Horita et al.*, 2002] suggest only insignificant changes in major ion concentrations (Na^+, Cl^-). By this way, the stability constants K_1 and K_2 are calculated as model variables considering the changing temperature and pressure conditions prevailing at depth L.

[18] The resulting carbonate ion concentrations (equation (6)) are used to constrain the rate of carbonate accumulation at the seafloor:

$$F_{BC} = k_{BC} \cdot \left(\frac{Ca \cdot CO_3}{K_{SP}} - 1 \right) \tag{8}$$

where Ca concentrations (Ca) are taken from brine inclusion data (Figure 1d) and the solubility product of calcite K_{SP} is again calculated as a function of temperature and pressure prevailing at depth L. The kinetic constant k_{BC} is set to a large value so that seawater is always maintained close to equilibrium with respect to calcite at depth L. The carbonate burial flux F_{BC} acts as a major sink for TC and CA (Table A5). Thus concentrations of dissolved carbonate species in the ocean are stabilized by a strong negative feedback.

[19] The partial pressure of CO_2 in surface waters (pCO_2^{SW}) is calculated as:

$$pCO_2^{SW} = \frac{K_1(TC_S - CA_S) + K_2(4CA_S - 8TC_S) + \sqrt{K_1(CA_S(K_1 - 4K_2)(CA_S - 2TC_S) + K_1TC_S^2)}}{2K_0(K_1 - 4K_2)} \tag{9}$$

where the total dissolved carbon concentrations and the carbonate alkalinity prevailing at the surface (CA_S, TC_S) are related to the corresponding values in the bulk ocean as:

$$\begin{aligned} TC_S &= TC - DC \\ CA_S &= CA - 0.1 \cdot \Delta C \end{aligned} \tag{10}$$

The concentration difference ΔC is due to the fixation of dissolved inorganic carbon in organic matter and biogenic carbonate by plankton and the export of biogenic particles into the interior of the ocean (the biological pump). This difference amounts to approximately 150 μM in the North Atlantic and 250 μM in the North Pacific [*Millero*, 1996] with an global average of approximately 200 μM. The corresponding difference in CA is about one order of magnitude smaller because the export flux of $CaCO_3$ from the euphotic zone is much smaller than the POC flux. The stability constants K_1, K_2 and K_0 (Henry constant) are again calculated as model variables considering the changing surface temperature (equation (5)), a pressure of 1 bar and a salinity of 35.

[20] The resulting pCO_2^{SW} values (equation (9)) are than used to determine the CO_2 exchange flux between surface ocean and atmosphere:

$$F_{EX} = k_{EX} \cdot \left(pCO_2^{SW} - pCO_2^{ATM} \right) \tag{11}$$

where pCO_2^{SW} and pCO_2^{ATM} are the partial pressures of CO_2 in the surface ocean and in the atmosphere, respectively, and k_{EX} is a kinetic constant. The difference in pCO_2 is due to the slow rate of gas exchange between surface waters and atmosphere. In today's ocean, the pCO_2 of surface waters is lower than the atmospheric value due to the anthropogenic increase in atmospheric CO_2 content [*Millero*, 1996]. The modern ocean thus serves as a sink for anthropogenic carbon. Before the onset of industrialization, the oceanic pCO_2 values were somewhat larger than the atmospheric pCO_2 value (280 μatm) and oceanic CO_2 degassed into the atmosphere [*Mackenzie et al.*, 2002]. The average ΔpCO_2 of the pre-industrial ocean was small (<10 μatm; *Maier-Reimer*, 1993) when compared to the huge changes in atmospheric pCO_2 over the Phanerozoic (up to 5000 μatm [*Berner and Kothavala*, 2001; *Royer et al.*, 2001]). Thus a large value is assigned to the kinetic constant k_{EX} so that pCO_2 in the atmosphere is always close to the surface water value. The solubility of CO_2 in seawater (K_0) is diminished at high temperatures so that a larger fraction of total CO_2 resides in the atmosphere under greenhouse conditions. A positive feedback is established

because surface temperature depends on the prevailing pCO_2^{ATM} level which is in turn controlled by the temperature-dependent air-sea exchange (Table A5). However, this feedback has only a small effect on the long-term evolution of temperature and pCO_2 because the total amount of CO_2 in oceans and atmosphere is regulated mainly by weathering and degassing processes.

[21] The pH of surface water (pH_s) is finally calculated from TC_s and CA_s as:

$$pH_S = -\log\left[\frac{K_1(TC_S - CA_S) + \sqrt{K_1(CA_S(K_1 - 4K_2)(CA_S - 2TC_S) + K_1TC_S^2)}}{2CA_S}\right] \quad (12)$$

considering again the changing surface temperatures and the temperature dependence of the stability constants.

2.4. Water Cycling

[22] The model considers mantle degassing, continental weathering, alteration of oceanic crust at high and low temperatures, serpentinization of mantle rocks, formation and melting of continental ice shields, and recycling of water at subduction zones. In the following, I briefly present the major changes of the model with respect to the previous approach [*Wallmann*, 2001b]. Complete lists of all fluxes, parameter values, and reservoirs considered in the simulation of the geological water cycle are given in the Appendix (Tables A3–A5).

[23] In the new coupled model of carbon and water cycling, many water fluxes are linked to the corresponding carbon fluxes. Thus the fixation of water in clay minerals (F_{WSH}) is related to the rate of silicate weathering (F_{WS}) as:

$$F_{WSH} = r_{WS} \cdot F_{WS} \quad (13)$$

where r_{WS} is the ratio of H_2O to CO_2 turnover during silicate weathering. Before the onset of large scale agriculture and anthropogenic erosion, water was fixed in clay minerals at a rate of $\approx 7 \times 10^{+18}$ mol H_2O Ma^{-1} [*Wallmann*, 2001b] while CO_2 was consumed at a rate of $\approx 7 \times 10^{+18}$ mol CO_2 Ma^{-1} [*Hansen and Wallmann*, 2003] so that the ratio r_{WS} is unity.

[24] Serpentinization was considered as an additional water uptake flux because recent work shows that mantle rocks are commonly exposed and serpentinized at slow-spreading ridges [*Schmidt and Poli*, 1998]. In contrast to the alteration of oceanic crust, the rate of water fixation during serpentinization (F_{SER}) is not proportional to the prevailing spreading rate, because slow spreading seems to favor the exposure of mantle rocks [*Charlou et al.*, 2002]. Thus F_{SER} is constant through time and equal to the current rate ($F_{SER}(Q)$) which amounts to approximately $20 \times 10^{+18}$ mol H_2O Ma^{-1} [*Wallmann*, 2001b]:

$$F_{SER} = F_{SER}(Q) \quad (14)$$

Large continental ice shields were formed during the late Permian to early Carboniferous glaciation and during the late Cenozoic. During these periods approximately 3–5% of the oceanic water masses were locked in continental ice. Gauss functions were used to prescribe the rates of freezing (F_{FR}) and melting (F_{MEL}) during these two major glaciations:

$$F_{FR} = A \cdot \left(e^{-\frac{(t-t_g)^2}{2 \cdot w^2}} + e^{-\frac{t^2}{w^2}}\right) \quad (15)$$

$$F_{MEL} = A \cdot \left(e^{-\frac{(t-t_g-w)^2}{2 \cdot w^2}}\right) \quad (16)$$

where the amplitude A and the width w were set to values of $122 \times 10^{+18}$ mol Ma^{-1} and 25 Ma, respectively. With this approach maximum ice masses of $3 \times 10^{+21}$ mol H_2O were produced corresponding to $\approx$4% of the current oceanic water mass ($1.37 \times 10^{+24}$ g = $76.1 \times 10^{+21}$ mol H_2O [*Broecker and Peng*, 1982]).

2.5. Simulation of Seawater $\delta^{18}O$ Values

[25] The modeling of marine $\delta^{18}O$ values is based on the simulation of the water cycle and the model presented in *Wallmann* [2001b]. The ^{18}O fluxes are linked to the corresponding water fluxes considering their isotopic composition. Thus the rate of $H_2^{18}O$ release via mantle degassing (F_{MH}^{18}) is related to the H_2O flux (F_{MH}) as:

$$F_{MH}^{18} = \Phi_M \cdot F_{MH} \quad (17)$$

where Φ_M is the mole fraction of ^{18}O in mantle-H_2O.

[26] The parameterization of isotopic exchange processes between seawater and oceanic crust was improved to maintain isotopic equilibrium between seawater and alteration products of oceanic crust. The isotopic exchange processes during alteration of the upper volcanic section at low temperatures (F_{EX}^{UP}) and of the deeper sections at high temperatures (F_{EX}^{DEEP}) are formulated as:

$$F_{EX}^{UP} = \left(\Phi_{BAS} - \Phi_{ALT}^{i}\right) \cdot r_{ALTO} \cdot F_{ALT} \quad \text{and} \quad F_{EX}^{DEEP} = \left(\Phi_{BAS} - \Phi_{SP}^{i}\right) \cdot r_{SPO} \cdot F_{SP} \tag{18}$$

where Φ_{BAS} is the mole fraction of ^{18}O in fresh oceanic crust, F_{ALT} and F_{SP} are rates of carbonate and water uptake during alteration of upper and lower oceanic crust, respectively, r_{ALTO} is the ratio between O turnover and $CaCO_3$ uptake in upper crust and r_{SPO} gives the ratio between O turnover and water uptake in deep crust. The mole fractions of ^{18}O in instantaneous products of alteration at low and high temperatures are given by:

$$\Phi_{ALT}^{i} = \frac{\alpha_{ALT} \cdot \Phi_{SW}}{\alpha_{ALT} \cdot \Phi_{SW} + 1 - \Phi_{SW}} \qquad \Phi_{SP}^{i} = \frac{\alpha_{SP} \cdot \Phi_{SW}}{\alpha_{SP} \cdot \Phi_{SW} + 1 - \Phi_{SW}} \tag{19}$$

Here, α_{ALT} (1.015) and α_{SP} (1.000) define the isotopic fractionation between seawater and alteration products at low and high temperatures, respectively. At high temperatures, the fractionation is strongly suppressed so that alteration products in deep crust attain the isotopic composition of seawater (Φ_{SW}).

2.6. Calculating the $\delta^{18}O$ Values of Marine Carbonate

[27] The vast $\delta^{18}O$ data set published by *Veizer et al.* [1999] is used in the evaluation of marine $\delta^{18}O$ values. This data set is based on the analysis of well-preserved brachiopods and belemnites which were carefully selected to exclude diagenetically altered samples. The isotopic composition of these samples is mainly controlled by seawater $\delta^{18}O$, temperature, and seawater pH.

[28] The isotopic fractionation factor between calcite and water ($\alpha_{c\text{-}w}$) defines the ratio of the isotope ratios in $CaCO_3$ and H_2O:

$$\alpha_{c-w} = \frac{\left({}^{18}O/{}^{16}O\right)_{calcite}}{\left({}^{18}O/{}^{16}O\right)_{H_2O}} \tag{20}$$

It depends on temperature [*Kim and O'Neil*, 1997] as:

$$1000 \cdot \ln \alpha_{c-w} = 18.03 \cdot \left(\frac{1000}{T}\right) - 32.42 \tag{21}$$

where T is temperature in °K.

[29] Moreover, the isotopic composition of carbonates is affected by the pH of ambient seawater. According to *Usdowski and Hoefs* [1993] and *Zeebe* [1999], the $\delta^{18}O$ of the precipitated carbonate reflects the isotopic composition of the quantity S which is defined as the sum of the carbonate anion, bicarbonate anion, and carbonic acid concentrations:

$$S = \left[CO_3^{2-}\right] + \left[HCO_3^{-}\right] + \left[H_2CO_3\right] \tag{22}$$

In other words, carbonate minerals are not only formed from carbonate anions but also from all other inorganic carbon species carrying the CO_3 group. Unfortunately, the isotopic fractionation factors between these three species and water are only known for a single temperature (19°C). Thus the impact of pH on the $\delta^{18}O$ of S and $CaCO_3$ can only be calculated for this temperature [*Zeebe and Wolf-Gladrow*, 2001]. Considering these data and their limitations, *Zeebe* [2001] proposed that the effect of seawater pH on the $\delta^{18}O$ values of marine carbonates can be estimated as:

$$\Delta^{18}O_{pH} = -1.42 \cdot \Delta pH \tag{23}$$

where ΔpH is the difference between the pH of ancient and modern seawater whereas $\Delta^{18}O_{pH}$ gives the change in the $\delta^{18}O$ values of marine carbonates due to the change in pH. Thus a decrease in pH from 8.2 to 7.2 induces an increase in $\delta^{18}O$ by 1.42‰.

[30] The isotopic composition of marine carbonates ($\delta^{18}O(CaCO_3)$ in ‰ PDB) is calculated as a function of seawater composition ($\delta^{18}O(SW)$ in ‰

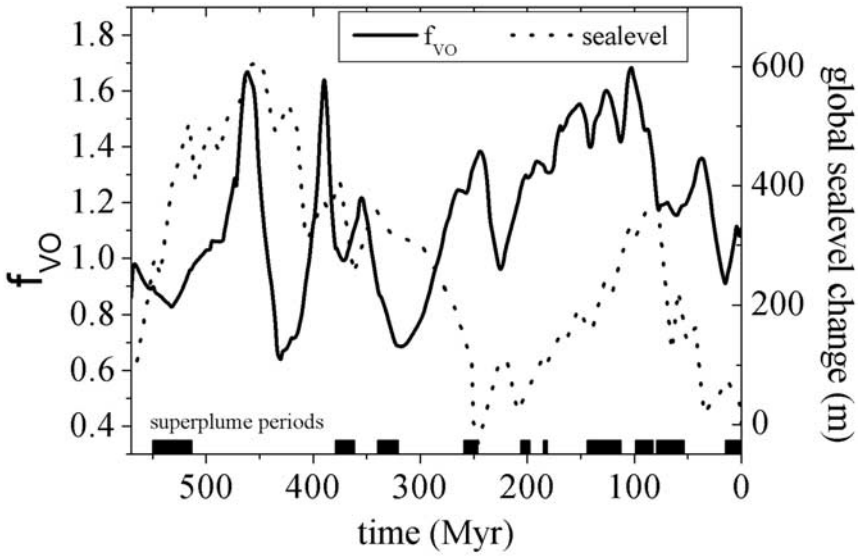

Figure 5. Change in volcanic/tectonic activity (f_{VO}) in the standard case as calculated from $^{87}Sr/^{86}Sr$ isotope data applying equations (1). The f_{VO} values are compared with the eustatic sea level curve of *Hallam* [1992]. Periods of superplume activity are shown as black bars at the base of the figure [*Abbott and Isley*, 2002].

SMOW), surface temperature (T_S in °C), and surface seawater pH (pH_S) as:

$$\delta^{18}O(CaCO_3) = \left(0.9391 \cdot \delta^{18}O(SW) + 939.1\right) \cdot Exp\left[\frac{18.03}{273.15 + T_S}\right] - 1000 - 1.42 \cdot \Delta pH_S \quad (24)$$

where the first term of the equation is derived from equation (21).

3. Results and Discussion

[31] First, a standard run is produced giving the best fit of model results to independent observations such as the marine $\delta^{18}O$ record, average Quaternary pCO_2 values and recent carbon masses in different sedimentary reservoirs. Subsequently, the controls on atmospheric pCO_2, average global surface temperature, and marine $\delta^{18}O$ are discussed using the results of the standard run and additional model runs with systematically varied parameter values.

3.1. Standard Case

[32] The change in volcanic/tectonic activity (f_{VO}) was determined applying a new kinetic approach (equations (1) and (2)) where the isotopic and chemical evolution of the model ocean is forced to follow the Sr/Ca values and $^{87}Sr/^{86}Sr$ trends observed in marine carbonates (Figure 1). In contrast to many previously applied isotopic mass balances, the new kinetic approach does not rely on questionable steady state assumptions. The kinetic equations (equations (1), (2) and (4)) are valid independent of the model formulation and the choice of input and output fluxes. They are very flexible tools which can be applied in any kind of model whereas conventional (isotopic) mass balances have to be reformulated for each specific set of fluxes.

[33] The resulting values (Figure 5) bear rather little resemblance with the eustatic sea level curve confirming that sea level change is not a valid proxy for changes in volcanic and tectonic activity. Some f_{VO} maxima coincide with maxima in sea level whereas others occur during periods of superplume activity [*Abbott and Isley*, 2002]. Thus maxima at 460 Myr and 100 Myr are accompanied by very high sea level stands whereas the maximum at 250 Myr coincides with the emplacement of the Siberian traps. Considering that ancient oceanic flood basalts and periods of enhanced spreading are not fully documented in the geolog-

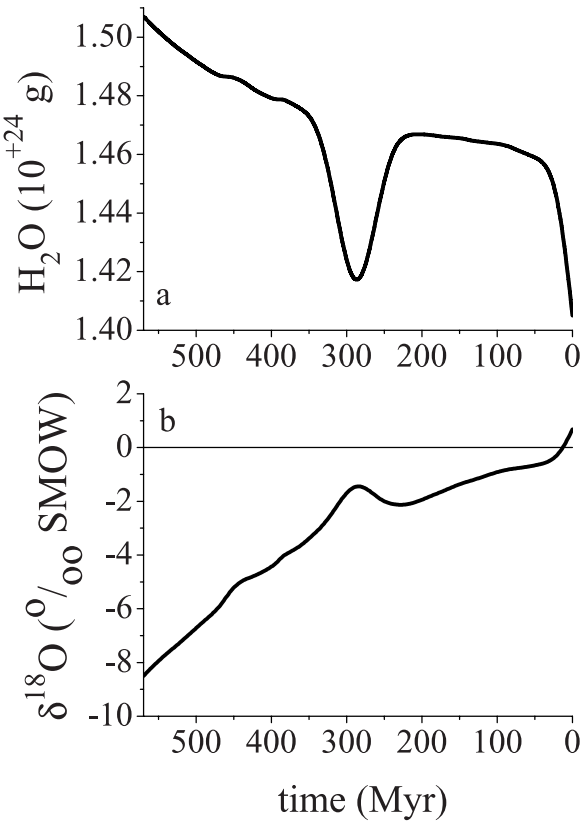

Figure 6. Change in mass and stable isotopic composition of seawater in the standard run. (a) Mass of liquid seawater in the oceans. (b) $\delta^{18}O$ value of seawater.

ical record, it is not surprising that periods of strong basaltic Sr release are not always accompanied by known magmatic events. The f_{VO} values derived above reflect the release of isotopically depleted Sr from weathering volcanic rocks deposited on the continents and basaltic basement rocks hydrothermally leached at submarine spreading centers. Thus they include the effects of volcanic activity both on land and at the seafloor. They can not be used to distinguish between plume-related intraplate volcanism and spreading/subduction related volcanism occurring at active plate margins. Thus changes in spreading/subduction rate might differ from the reconstructed f_{VO} values during periods of intense intraplate volcanism. This limitation should be noted in the following. Nevertheless, the changes in volcanic/tectonic activity reconstructed here from the marine $^{87}Sr/^{86}Sr$ record (Figure 5) are arguably more valid than previously used proxies.

[34] In the standard case, the amount of liquid water in the oceans decreases steadily over time (Figure 6a) because the subduction of water into the mantle proceeds at a higher rate than the degassing of the mantle [*Wallmann*, 2001b]. Moreover, the seawater mass is diminished during major icehouse periods due to the formation of massive continental ice shields. Starting with the strongly negative $\delta^{18}O$ suggested by the marine carbonate record, seawater $\delta^{18}O$ values increase continuously toward the modern value (Figure 6b). The rate of increase is lower in the standard case than in previous model simulations [*Wallmann*, 2001b] because the rate of upper crust alteration at low temperature now depends on the amount of pelagic carbonate sediments deposited at the seafloor. As pelagic carbonates have been formed only since the beginning of the Mesozoic, Paleozoic ridge flanks were covered with a much thinner sedimentary apron allowing for a more intense hydrothermal circulation and higher rates of low-temperature alteration of upper oceanic crust. The effect of a missing sediment cover on upper crustal $\delta^{18}O$ values can be seen at ODP hole 417A situated on a basement hill. Here, outcropping crustal rocks were fully exposed to seawater for ~20 Myr and the average $\delta^{18}O$ value of the upper 100 m of the crustal section was enhanced to ~+25‰ (SMOW) due to pervasive fluid flow and alteration [*Alt*, 2003]. In contrast, ridge flanks covered with carbonate sediments attain a much lower $\delta^{18}O$ (typically +8–+10‰ [*Alt*, 2003]) because fluid flow and alteration are suppressed by the impermeable sedimentary apron. Thus it seems to be possible that the very low $\delta^{18}O$ values of Paleozoic and Precambrian carbonates [*Shields and Veizer*, 2002] reflect strong isotopic depletion of ambient seawater caused by intense low temperature alteration of exposed ridge flanks.

[35] The pCO_2 values calculated in the standard case (Figure 7a) differ strongly from previous model results [*Berner and Kothavala*, 2001; *Hansen and Wallmann*, 2003; *Wallmann*, 2001a]. This deviation is mainly due to the impact of galactic cosmic radiation (GCR) on surface temperature which is considered in the new model for the first time. Thus strong maxima in pCO_2

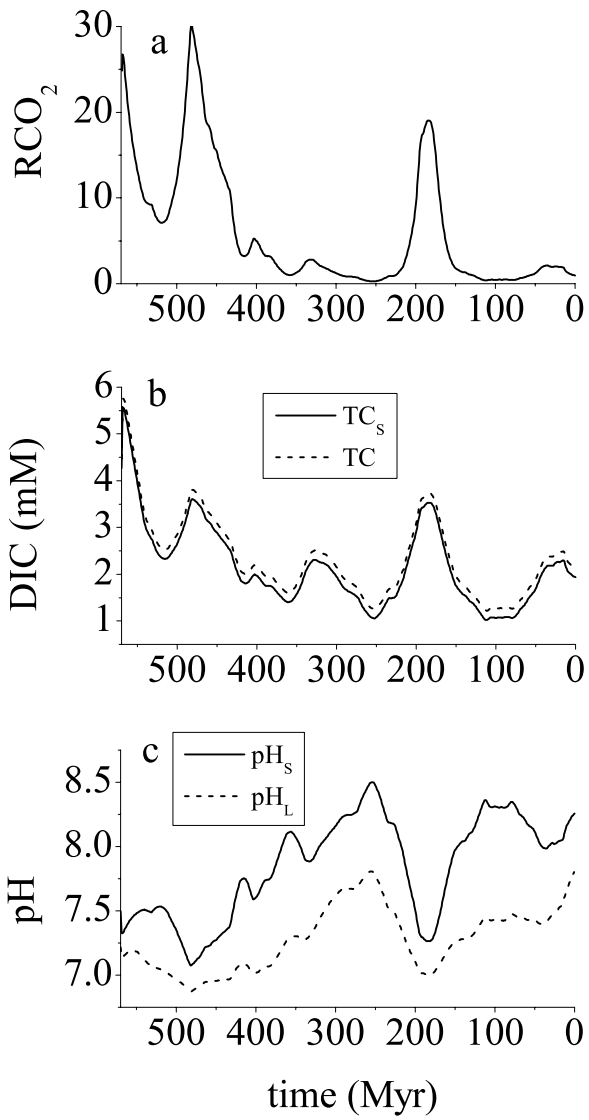

Figure 7. Change in atmospheric pCO_2, dissolved inorganic carbon concentration and seawater pH in the standard case. (a) Atmospheric pCO_2 normalized to the Quaternary value (230 μatm). (b) Dissolved inorganic carbon in surface waters (TC_S) and in the bulk ocean (TC). (c) Seawater pH values in surface water (pH_S) and at the calcite saturation depth (pH_L).

occur during periods of high GCR (Figure 3) because the presumed cooling effect of GCR induces a decrease in silicate weathering rates and thus an increase in pCO_2. The negative feedback between surface temperature, silicate weathering rate and pCO_2 is believed to be responsible for the long-term stability of global climate [*Walker et al.*, 1981] and acts here to compensate for the cooling induced by GCR.

[36] Concentrations of total dissolved inorganic carbon (Figure 7b) correlate with the pCO_2 trends (Figure 7a) and are also modulated by the prescribed dissolved Ca concentrations (Figure 1d). Surface concentrations are always lower than the bulk ocean concentrations due to the prescribed concentration gradients (equation (10)). Seawater pH values reflect the evolution of atmospheric pCO_2 and dissolved inorganic carbon concentrations. They are low during periods of enhanced pCO_2 and high during major icehouse periods. The pH contrast between surface water and deep water

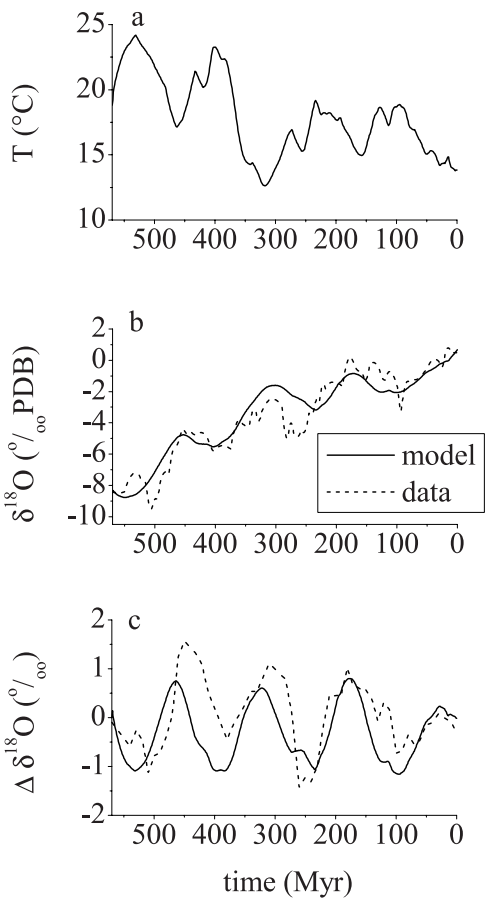

Figure 8. Change in surface temperature and marine $\delta^{18}O$ values in the standard run. (a) Average global surface temperature. (b) $\delta^{18}O$ values of marine carbonates as calculated in the model and measured in marine carbonate fossils [*Veizer et al.*, 1999]. (c) Difference between the $\delta^{18}O$ values of marine carbonates (in ‰ PDB) and coeval seawater (in ‰ SMOW) as calculated in the model (solid line) and by detrending of the running means (step 10 Myr, window 50 Myr) of the $\delta^{18}O$ carbonate data [*Veizer et al.*, 2000].

changes in time due to the varying depth of the calcite saturation level (Figure 4d).

[37] Surface temperatures predicted by the model are in general agreement with the trends observed in independent paleoclimatic reconstructions [*Crowley and Berner*, 2001; *Frakes et al.*, 1992]. Thus they show cool icehouse conditions for the late Cenozoic and the late Permian - early Carbonaceous glaciations (Figure 8a). Temperatures decrease during phases of high GCR but the amplitudes of temperature change are heavily affected by the carbon cycle. Thus the cooling during the mid-Mesozoic is rather modest because high rates of volcanic/tectonic activity allow for a built-up of high pCO_2 values compensating effectively for the cooling through GCR-induced cloud formation. In contrast, the effects of GCR are further enhanced by carbon cycling processes during the late Permian - early Carbonaceous glaciation because pCO_2 values are diminished by enhanced organic carbon burial and plant-induced weathering processes [*Berner*, 1997].

[38] The marine $\delta^{18}O$ values follow the trends observed in the geological record [*Veizer et al.*, 1999] and show a very strong correlation with the GCR flux (Figures 8b and 3). They reflect changes in the isotopic composition of seawater, surface temperature, and surface water pH.

3.2. Controls on Atmospheric pCO_2

[39] Systematic parameter variations showed that RCO_2 values (atmospheric pCO_2 normalized to the Quaternary value of 230 μatm) are mainly controlled by the spread and evolution of land plants [see also *Berner*, 1997], and by the intensity of volcanic/tectonic activity and GCR. The RCO_2 trends in the standard run are rather close to those reconstructed from paleo-sols and other proxy data (Figure 9a) [*Royer et al.*, 2001]. The model reproduces the strong RCO_2 peak observed in Jurassic samples whereas the GEOCARB models predict much lower Jurassic values [*Berner*, 1991a, 1994; *Berner and Kothavala*, 2001].

[40] When the GCR effect on temperature is completely suppressed ($\Delta_{COS} = 0$ in equation (5)), RCO_2 values change drastically and the resulting trends are similar to those observed in the GEOCARB III model (Figure 9b). The strong Jurassic peak is diminished whereas Cambrian, Devonian and Cretaceous RCO_2 values increase considerably. These changes are induced by the impact of GCR on temperature-dependent chemical weathering rates. During periods of low GCR (Cambrian, Devonian, Cretaceous, Triassic), surface temperatures increase due to the diminished cloudiness at low altitudes so that weathering is accelerated and RCO_2 is removed from the atmosphere. In contrast, high GCR intensity during the Ordovician, Carboniferous, and Jurassic (Figure 3) reduces

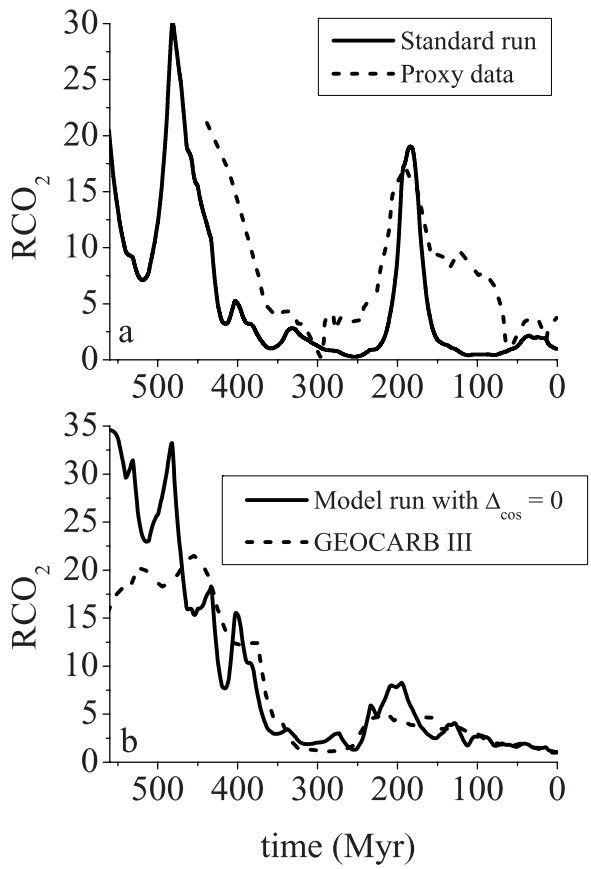

Figure 9. Change in normalized atmospheric pCO_2. (a) Results of the standard run compared to proxy data. The dotted proxy line is the running mean derived from paleosol and other proxy data considering recalculated values for the Permian and Carboniferous [*Royer et al.*, 2001]. (b) Model output without GCR effect on temperature compared to the GEOCARB III standard run.

surface temperature due to enhanced cloudiness so that less CO_2 is consumed in weathering processes.

[41] Rates of chemical weathering do not only depend on temperature but also on precipitation and the availability of meteoric water. It seems to be possible that reduced cloudiness during low GCR periods induces lower rates of precipitation which could than diminish weathering rates compensating for the effect of enhanced temperature. However, a number of studies show that low-altitude cloud coverage (below ~3.2 km altitude) over the modern oceans is significantly affected by GCR [*Marsh and Svensmark*, 2000b; *Shaviv*, 2002b; *Yu*, 2002] so that more water is evaporated and transported to the continents at low GCR intensity [*Kniveton and Todd*, 2001]. The more efficient water transfer might enhance precipitation on land and continental run-off and thereby chemical weathering rates during low GCR periods. However, the effects of GCR on surface temperature and the hydrological cycle are not fully understood and need to be investigated in more detail using general circulation modeling and other approaches.

[42] The new model predicts higher Jurassic RCO_2 values than the GEOCARB III model even in the absence of GCR effects (Figure 9b). This difference is caused by higher rates of volcanic/tectonic activity reconstructed from the strontium isotope data. The marine $^{87}Sr/^{86}Sr$ record reaches a minimum during the late Jurassic (Figure 1a) implying high rates of volcanic activity at the seafloor or on land whereas the eustatic sea level is not particularly elevated during this period (Figure 5). Therefore the sea level-based GEOCARB models predict a modest CO_2 release from the mantle whereas the new model produces enhanced Jurassic degassing rates. The proxy record shows a rather good correlation between high pCO_2 (Figure 9a; *Royer et al.*, 2001) and low marine $^{87}Sr/^{86}Sr$ values [*Veizer et al.*, 1999] over the Mesozoic and Cenozoic implying that strontium isotope data can be used as a proxy for volcanic activity and CO_2 release. Paleozoic pCO_2 values are strongly affected by the rise of land plants so that Paleozoic trends in pCO_2 reflect the increasing efficiency of chemical weathering rather than changes in the volcanic CO_2 supply. The new model also predicts higher Cambrian pCO_2 values than the GEOCARB III model. This difference is caused by lower rates of physical erosion applied in the new model. In GEOCARB modeling, erosion rates are reconstructed using the marine $^{87}Sr/^{86}Sr$ record whereas the new model relies on rates of terrigenous sedimentation taken from Ronov's database (Figure 2a). Overall, the rather good agreement between the two models (Figure 9b) is encouraging and implies that model results are rather well constrained by $\delta^{13}C$ and $^{87}Sr/^{86}Sr$ isotope records and GEOCARB weathering equations applied in both models.

3.3. Controls on Surface Temperature

[43] Temperature changes caused by the aging sun, paleogeographic evolution, and GCR intensity are implemented as external forcing to the model (equation (5), Figure 10a). During the Cambrian, solar radiation was much weaker than today so that surface temperatures would have been 7.4°C lower at a modern RCO_2 level and geographic configuration [*Berner and Kothavala*, 2001]. In contrast, paleogeographic change promoted a slow cooling of the Earth over the Phanerozoic [*Berner and Kothavala*, 2001] whereas GCR fluctuations might have inducted periodic changes between warm and cold periods [*Shaviv and Veizer*, 2003]. RCO_2-induced temperature changes are not prescribed to the model but are calculated as an internal variable affected by carbon cycling processes and by externally driven temperature change (Figure 10b). Moreover, the parameter Γ relating RCO_2 and surface temperature (equation (10)) is allowed to change through time (Figure 4b) to account for the temperature and albedo effects of large continental ice shields waning and waxing over the Phanerozoic [*Berner and Kothavala*, 2001].

[44] The overall temperature change resulting from the linear superposition of all internal and external effects (calculated according to equation (10)) reflects mainly the response of the carbon cycle to varying insolation and GCR fluxes (Figure 10c). Because of the negative feedback rooted in the temperature-dependence of silicate weathering

[*Walker et al.*, 1981], pCO_2 changes tend to oppose and diminish externally driven temperature variations. Thus RCO_2 values are high during periods of strong GCR and tend to decrease over the Phanerozoic due to the continuous increase in solar radiation. Additional pCO_2 and temperature changes are driven by carbon cycling processes such as chemical weathering and mantle degassing which are related to the evolving biogeochemical and volcanic/tectonic Earth systems.

[45] In the standard run, Phanerozoic climate change is clearly affected by GCR variations. Thus temperatures tend to be low during high GCR periods (marked as gray bars in Figure 10) and high during low GCR periods. However, the GCR effects on temperature are strongly overprinted by RCO_2 changes. The partial pressures of CO_2 are controlled by volcanic/tectonic and biogeochemical processes acting on the carbon cycle and by radiation-induced temperature changes affecting the rates of silicate weathering. The latter process induces a dampening of radiation-controlled climate change. The overall climate evolution thus reflects both external forcing via solar and cosmic radiation and internal forcing related to the evolving carbon cycle.

3.4. Controls on Marine $\delta^{18}O$ Values

[46] The isotopic composition of marine carbonates depends on the $\delta^{18}O$ of ambient seawater, on seawater pH and surface temperature whereas the difference between carbonate and seawater $\delta^{18}O$ ($\Delta\delta^{18}O$) is a function of temperature and pH, only. The contributions of the latter two parameters to the Phanerozoic trends in $\Delta\delta^{18}O$, depicted in Figure 11a and 11b, reflect the temperature and pH changes shown in Figure 10c and 7c, respectively. Thus warm periods are marked by negative $\Delta\delta^{18}O_T$ values while acidic conditions in surface waters induce strongly positive $\Delta\delta^{18}O_{pH}$ values. As enhanced partial pressures of CO_2 tend to increase temperature and decrease pH, the overall effect of RCO_2 on $\Delta\delta^{18}O$ is rather small. Intense GCR induces a cooling of surface temperature, resulting in an increase in $\Delta\delta^{18}O_T$ and a decrease in pH causing an increase in $\Delta\delta^{18}O_{pH}$, due to diminished rates of silicate weathering and enhanced RCO_2 values. In other words, GCR has a very significant effect on marine $\Delta\delta^{18}O$ values because both temperature and pH dependent $\Delta\delta^{18}O$ values ($\Delta\delta^{18}O_T$ and $\Delta\delta^{18}O_{pH}$) are enhanced during periods of intense GCR (Figure 11). Hence the marine $\delta^{18}O$ record is remarkably insensitive toward RCO_2 changes but very sensitive with respect to GCR changes.

[47] The marine $\delta^{18}O$ record gives a somewhat distorted picture of Phanerozoic climate evolution and the forcing of climate change if the pH effect on the carbonate $\delta^{18}O$ value is neglected. The very strong correlation between GCR and marine $\delta^{18}O$ and the poor correlation between RCO_2 and $\delta^{18}O$ seems to imply that Phanerozoic climate change is not driven by RCO_2 but rather by GCR changes [*Shaviv and Veizer*, 2003]. However, when the pH effect and the contrasting sensitivities of marine $\delta^{18}O$ with respect RCO_2 and GCR are considered, a different picture emerges showing that RCO_2 and GCR are the two major and equally important climate drivers.

[48] The periodic variations seen in the carbonate record are remarkably well reproduced in the standard run whereas the model run without GCR produces $\Delta\delta^{18}O$ trends which are not consistent with the carbonate isotope data (Figures 8 and 11). The model was run repeatedly applying a large number of different parameter values but the marine $\delta^{18}O$ data were only recaptured considering the effect of GCR on surface temperature. Considering that the periodicity seen in the marine $\delta^{18}O$ data is statistically robust and is based on thousands of measurements in well preserved brachiopods [*Veizer et al.*, 1999], the model strongly suggests that GCR does indeed affect global climate and carbon cycling. In contrast to previous models [*Berner*, 1994; *Berner and Kothavala*, 2001], the new model presented here reproduces and considers all available isotope data [*Veizer et al.*, 1999] including the previously neglected $\delta^{18}O$ record.

[49] In the modern ocean, the $\delta^{18}O$ values of surface waters (and brachiopods) show a strong latitudinal variation which is well correlated with salinity due to evaporation and precipitation of

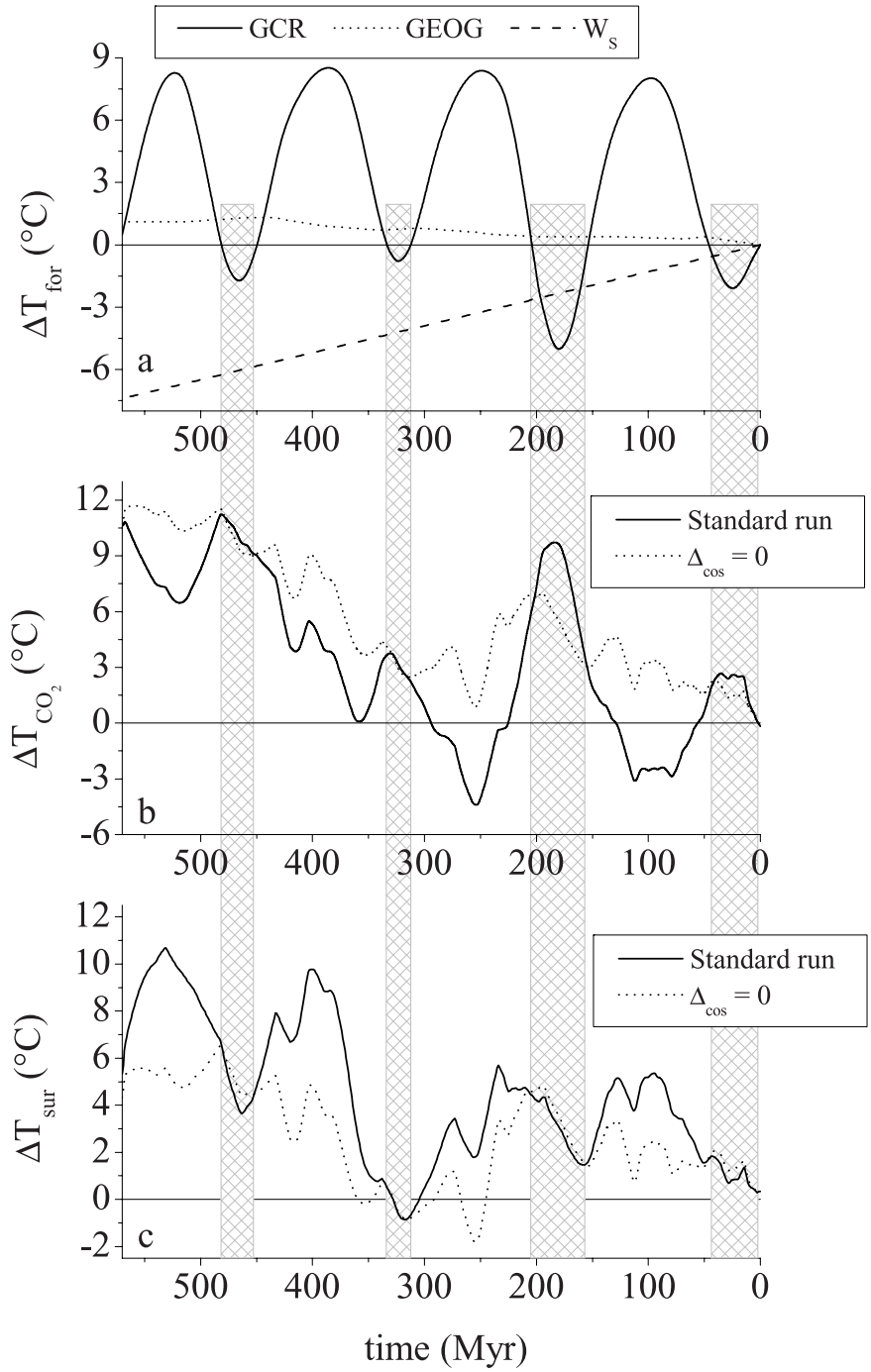

Figure 10. Evolution of average global surface temperatures over the Phanerozoic. Temperatures are plotted as difference to the Quaternary value (13.5°C). Hatched bars indicate periods of high GCR intensity. (a) Prescribed temperature changes considering the effects of sun aging (W_S), paleogeography (GEOG), and GCR. (b) Temperature changes inducted by RCO_2 in the standard model run and a model run without GCR forcing. (c) Surface temperature changes resulting from external forcing (W_S, GEOG, GCR) and internal RCO_2 effects as calculated in the standard model run and a model run without GCR forcing.

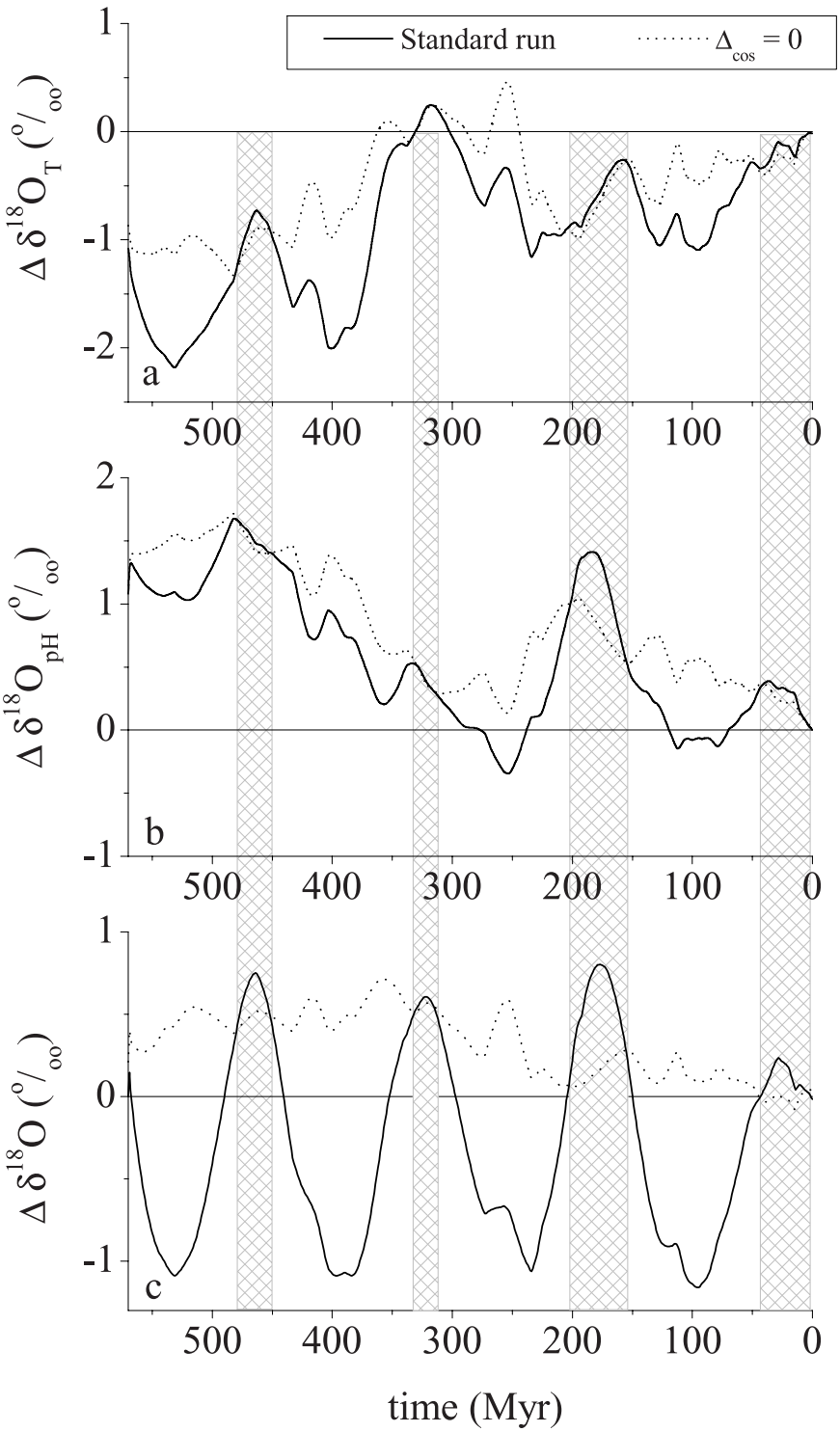

Figure 11. Difference between the $\delta^{18}O$ values of marine carbonates (in ‰ PDB) and coeval seawater (in ‰ SMOW) over the Phanerozoic. Hatched bars indicate periods of high GCR intensity. Solid lines give the results of the standard run whereas dotted lines indicate the results of a model run without GCR forcing. (a) Temperature-related $\delta^{18}O$ differences calculated according to equation (21). (b) $\delta^{18}O$ differences caused by pH change (equation (23)). (c) Overall $\delta^{18}O$ differences resulting from both temperature and pH effects (equation (24)).

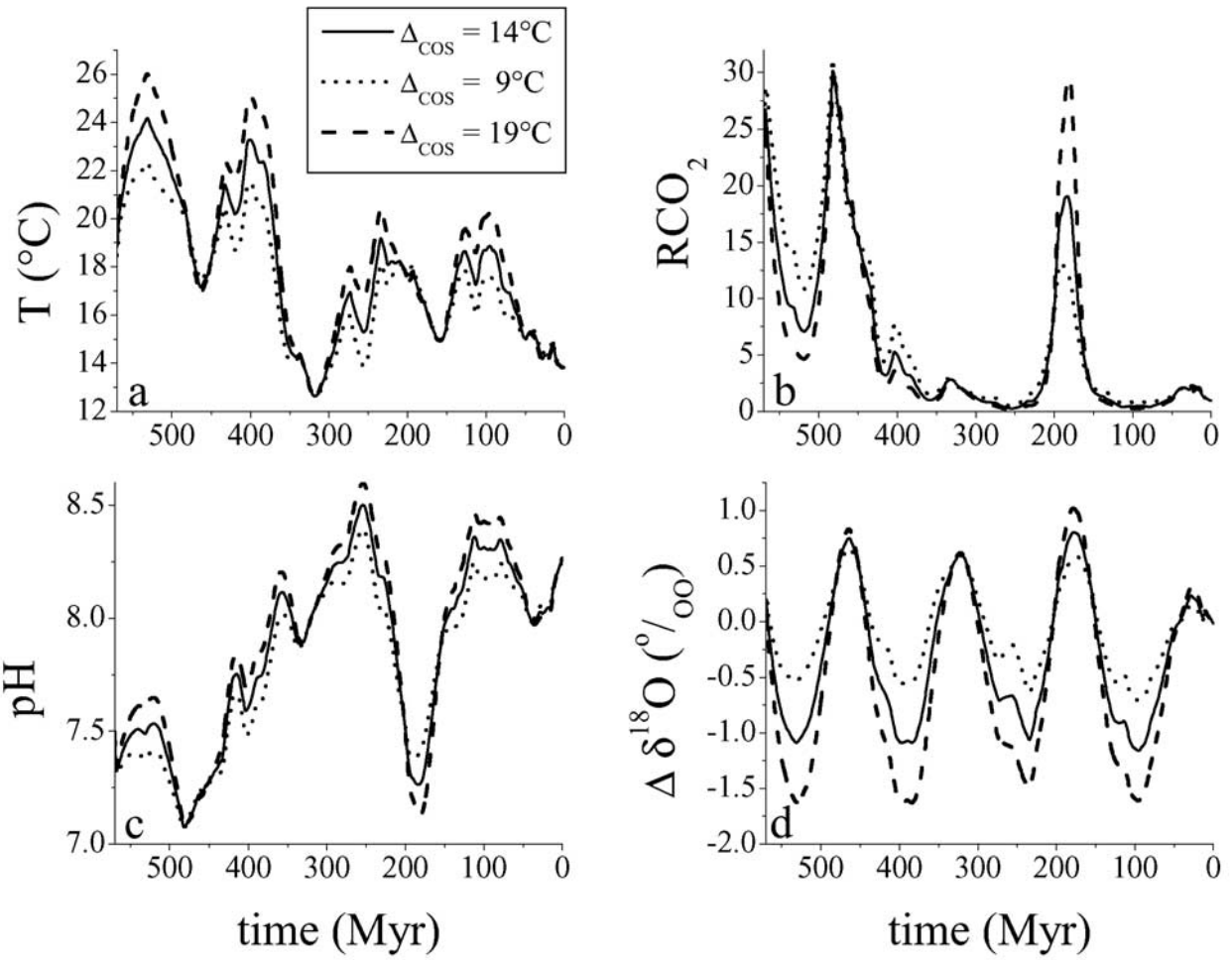

Figure 12. Effects of galactic cosmic radiation on climate, carbon cycling and marine $\delta^{18}O$ values. The model was run with three different values of the parameter Δ_{COS} defining the extent of the GCR effect on global average surface temperature via cloud formation. A_{COS} was varied between 9°C (weak effect of GCR on temperature), 14°C (standard case) and 19°C (strong effect of GCR on temperature). (a) Global average surface temperature. (b) Atmospheric partial pressure of CO_2 normalized to the Quaternary value (230 μatm). (c) pH in surface water. (d) Difference between the $\delta^{18}O$ values of marine carbonates (in ‰ PDB) and coeval seawater (in ‰ SMOW).

meteoric water [*Brand et al.*, 2003]. Thus saline water masses with high $\delta^{18}O$ values are usually found at low latitudes where net evaporation prevails. In contrast, low-salinity waters with low and negative $\delta^{18}O$ values are abundant at high latitudes due to net precipitation. The fossil brachiopods used in the reconstruction of marine $\delta^{18}O$ values dwelled mainly in low-latitude surface waters [*Veizer et al.*, 1999]. A number of studies show that low cloud cover (below ~3.2 km altitude) over the modern oceans is significantly enhanced during periods of high cosmic radiation [*Marsh and Svensmark*, 2000b; *Shaviv*, 2002b; *Yu*, 2002]. The correlation is especially well expressed at low and mid latitudes [*Kniveton and Todd*, 2001; *Marsh and Svensmark*, 2000b]. Moreover, the precipitation efficiency is enhanced so that moisture is more efficiently converted into precipitation under high cosmic radiation [*Kniveton and Todd*, 2001]. Thus it seems to be likely that the low-latitude ocean experienced less net evaporation during periods of enhanced GCR flux. This would have induced lower salinities and lower $\delta^{18}O$ values for the water masses building the habitat of ancient brachiopods. Thus the strong increase observed in the $\delta^{18}O$ values of brachiopod fossils originating from periods of enhanced GCR [*Shaviv and Veizer*, 2003] is not due to changes in the latitudinal gradient of

seawater $\delta^{18}O$ but rather reflects changes in temperature and seawater pH.

3.5. Effects of GCR on Climate, Atmospheric pCO_2, Seawater pH, and Carbonate $\delta^{18}O$ Values

[50] The effect of GCR on surface temperature (Δ_{COS}) was varied in a number of model runs to explore the effect of the GCR - temperature coupling intensity on Phanerozoic climate change, carbon cycling and marine $\delta^{18}O$ trends (Figure 12). An increase in Δ_{COS} produces a strong increase in temperature during phases of low GCR flux. Presumably, the decrease in GCR reduces the cloud cover at low altitudes so that surface temperatures increase for a given pCO_2 and insolation. The temperatures predicted for cool periods are not strongly affected by the Δ_{COS} variable because the Earth receives currently a high dose of cosmic radiation and GCR changes are calculated with respect to this high modern baseline value (Figure 3).

[51] RCO_2 varies as a consequence of GCR-driven temperature change. The Jurassic value is extremely sensitive because both GCR forcing (Figure 3) and volcanic/tectonic activity (Figure 5) attained a maximum during this period. If the Jurassic cooling presumably induced by high GCR is enforced by a large Δ_{COS} value, RCO_2 strongly increases due to the negative weathering feedback. The best fit to the proxy record (Figure 9a) is achieved in the standard run (Figure 12b). Trends in seawater pH mirror RCO_2 changes because the pH is lowered at high RCO_2 levels (Figure 12c). Carbonate $\delta^{18}O$ values are affected by both temperature and pH. The amplitude of $\delta^{18}O$ change is considerably enhanced when GCR is assumed to have a strong effect on surface temperature (Figure 12d). The standard run gives again the best fit to the proxy data (Figure 8c). Thus the Δ_{COS} value derived from modern data [*Shaviv*, 2002a] seems to be valid also for long-term climate change.

3.6. Reconstructing Phanerozoic Climate Change

[52] The climate evolution calculated in the standard run of the new model (Figure 13d) compares

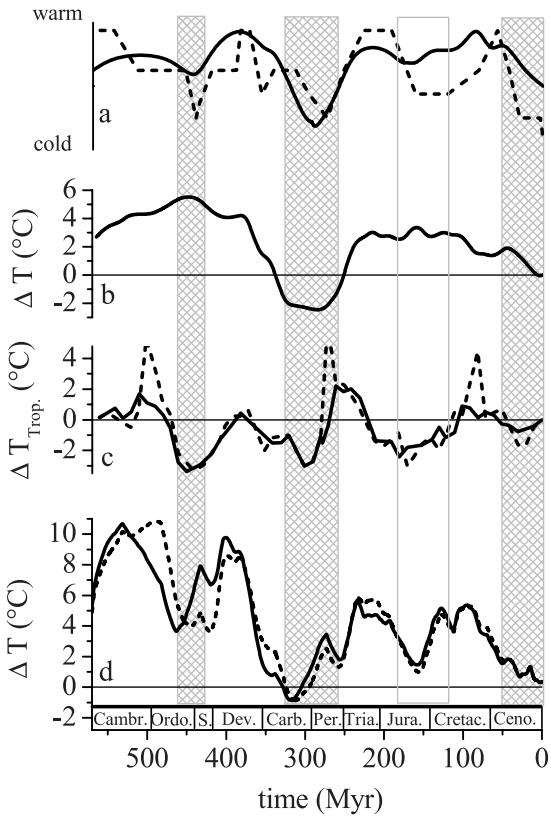

Figure 13. Phanerozoic climate evolution. (a) Relative change in global surface temperature as derived from sedimentary observations (solid line; *Frakes et al.*, 1992) and other geological proxies including coal, evaporates, tillites, calcretes, bauxites, kaolins, and fossils (broken line; *Boucot and Gray*, 2001). (b) Change in global average surface temperature calculated in the standard run of the GEOCARB III model [*Berner and Kothavala*, 2001]. (c) Change in tropical surface temperature derived from the marine $\delta^{18}O$ record [*Veizer et al.*, 2000]. The solid line is a running mean with a step of 10 Myr and a window of 50 Myr while a window of only 20 Myr was used for the broken line. (d) Change in global average surface temperature as calculated in the standard run (solid line) and in a model run with tuned cosmic radiation fluxes (broken line). The tuned fluxes were taken from *Shaviv and Veizer* [2003]. They were derived by fine tuning of the GCR periodicity within the GCR reconstruction error [*Shaviv and Veizer*, 2003]. The lower bar shows the geological periods according to the timescales of *Harland et al.* [1990] and *Gradstein et al.* [1995]. Hatched bars indicate cool periods according to *Frakes et al.* [1992]. The open vertical bar indicates the controversial Jurassic to early Cretaceous period where some authors postulate very warm surface conditions [*Crowley and Berner*, 2001] while others suspect moderate cooling [*Frakes et al.*, 1992; *Podlaha et al.*, 1998; *Boucot and Gray*, 2001]. Temperature changes (ΔT) are given with respect to the average Quaternary surface temperature of 13.5°C.

favorably with the proxy record (Figure 13a). The two major Phanerozoic glaciations during the late Carboniferous to early Permian and the late Cenozoic are well reproduced by the model. The late Jurassic to early Cretaceous appears as a moderately cool period as also suggested by most proxy data [*Frakes et al.*, 1992; *Podlaha et al.*, 1998; *Boucot and Gray*, 2001]. GEOCARB modeling predicts the highest temperatures of the entire Mesozoic for this period (Figure 13b) while temperatures significantly below the present level (Figure 13c) were derived from the $\delta^{18}O$ record [*Veizer et al.*, 2000; *Wallmann*, 2001b]. The modeling presented in this paper strongly suggests that these previous interpretations of the Jurassic to early Cretaceous temperature record are not correct because the GCR effect was not considered in the GEOCARB modeling while the pH effect on the isotopic composition of carbonates was ignored in the interpretation of the marine $\delta^{18}O$ record.

[53] The model was also run applying a different GCR flux evolution as forcing (Figure 13d, broken line). These GCR fluxes have been tuned within the GCR reconstruction error by *Shaviv and Veizer* [2003] to fit the paleo-climatic record conserved in marine sediments (red curve in their Figure 2). The model run predicts correctly a temperature minimum for the Ordovician - Silurian glaciation while the standard run produced a temperature minimum prior to the onset of the glaciation (Figures 13a and 13d). Thus the Paleozoic GCR record applied in the standard case might be somewhat distorted and the fine-tuned GCR evolution seems to give better results for this period. Previous reconstructions predicted either the highest (Figure 13b) or the lowest (Figure 13c) temperatures of the entire Phanerozoic for the Ordovician - Silurian glaciation. Both interpretations seem to be at odds with the sedimentary record (Figure 13a) suggesting a minor glaciation extending over only a rather short period of time (Figure 13a). Here again, the new model-based reconstruction, considering the GCR and pH effects, seems to be more realistic and consistent with the geological record.

[54] The new model predicts high surface temperatures for the Cambrian, Devonian, Triassic, and Cretaceous in good correspondence to the geological record [*Frakes et al.*, 1992; *Boucot and Gray*, 2001]. All of these warm periods are marked by a rather low GCR intensity (Figure 3) while the pCO_2 values were variable at moderately high to very low levels (Figure 9). Apparently the warm climate mode is not primarily caused by greenhouse gas forcing as usually assumed [*Fischer*, 1981] but by reduced cloud coverage induced by low GCR levels. The clear skies of these warm periods may thus be imagined as being covered mainly by optically thin high-altitude rather than thick low-altitude clouds. The two very cold periods during the late Carboniferous to early Permian and the late Cenozoic are marked by high GCR fluxes and low pCO_2 values. The major glaciations occurring during these periods are the result of carbon cycling processes causing a draw-down of atmospheric CO_2 [*Berner*, 1992; *Wallmann*, 2001a] and a coevally prevailing dense cloud cover at low-altitudes induced by strong GCR fluxes. The two moderately cool periods during the Ordovician - Silurian and Jurassic - early Cretaceous are characterized by both high pCO_2 and GCR levels so that greenhouse warming compensated for the cooling effect of low altitude clouds.

4. Conclusions

[55] The new model presented in this paper is able to reproduce not only the trends observed in the marine $\delta^{13}C$ and $^{87}Sr/^{86}Sr$ records but also the marine $\delta^{18}O$ data [*Veizer et al.*, 1999] which have been ignored in previous models of Phanerozoic carbon cycling and climate change. The $\delta^{18}O$ data are reproduced by the model only when GCR is allowed to have a strong effect on surface temperature. Considering that the periodicity seen in the enormously large marine $\delta^{18}O$ database is statistically robust [*Veizer et al.*, 1999], the model confirms that GCR does indeed affect Phanerozoic climate change [*Shaviv*, 2002a].

[56] Global carbon cycling is also affected by cosmic radiation because GCR-induced cooling reduces the CO_2 consumption via silicate weathering. The pCO_2 level increases as a response to

reduced weathering and can reach very high values if sufficient CO_2 is provided by volcanic and metamorphic processes. Thus the strong Jurassic pCO_2 maximum reconstructed from paleosol data [*Royer et al.*, 2001] was probably caused by coeval maxima in volcanic activity and GCR.

[57] Atmospheric pCO_2 enhances surface temperatures but reduces the pH of seawater. The warming causes a decrease in carbonate $\delta^{18}O$ while the coeval decrease in pH induces a rise in $\delta^{18}O$. Thus pCO_2 changes exert two opposing effects on carbonate $\delta^{18}O$ values so that the marine $\delta^{18}O$ record is remarkably insensitive toward pCO_2 change. In contrast, GCR induces a decrease in surface temperature and pH due to enhanced cloud coverage and diminished weathering rates. Both changes induce an increase in carbonate $\delta^{18}O$ so that the marine $\delta^{18}O$ record is very sensitive toward GCR change. Thus the very strong correlation observed between GCR and marine $\delta^{18}O$ and the poor correlation between RCO_2 and $\delta^{18}O$ do not imply that Phanerozoic climate change is almost exclusively driven by GCR changes [*Shaviv and Veizer*, 2003]. Considering the contrasting sensitivities of marine $\delta^{18}O$ with respect to RCO_2 and GCR, a different picture emerges showing that pCO_2 and GCR are the two major and equally important climate drivers.

[58] Warm periods (Cambrian, Devonian, Triassic, Cretaceous) are characterized by low GCR and variable pCO_2 levels. Thus the warm climate mode is not primarily caused by greenhouse gas forcing as usually assumed [*Fischer*, 1981] but by reduced cloud coverage induced by low GCR levels. The two major Phanerozoic glaciations during the late Carboniferous to early Permian and the late Cenozoic are the result of carbon cycling processes causing a draw-down of atmospheric CO_2 [*Berner*, 1992; *Wallmann*, 2001a] and a coevally prevailing dense cloud cover at low-altitudes induced by strong GCR fluxes. The two moderately cool periods during the Ordovician - Silurian and late Jurassic - early Cretaceous are characterized by both high pCO_2 and GCR levels so that greenhouse warming compensated for the cooling effect of low altitude clouds.

[59] Phanerozoic climate change seems to be driven and regulated by galactic, solar, and terrestrial processes. Cosmic radiation, produced mainly by exploding large stars (supernova events) in the spiral arms of the galaxy, probably supports cloud formation at low altitudes while solar irradiance increases continuously due to the ageing of the sun. Galactic and solar climate effects are moderated by the terrestrial carbon cycle. The periodicity and phase of climate change seem to be determined by the passage of the solar system through the spiral arms of the galaxy while the amplitude of temperature change is heavily affected by carbon cycling processes and pCO_2 variations.

[60] Holocene climate change seems to be affected by cosmic radiation, as well, because the production rate of cosmogenic isotopes (^{14}C, ^{10}Be) shows a very good correlation with proxy data from various climate archives [*Bond et al.*, 2001; *Neff et al.*, 2001; *Hu et al.*, 2003; *Niggemann et al.*, 2003]. It is generally believed that rapid changes in GCR indicated by cosmogenic isotope proxies are caused by changes in solar activity. Hence the observed climate effects may be due to GCR-induced cloud formation or could be caused by changes in solar irradiance which are very small in the visible range but quite substantial on shorter UV wavelengths [*Foukal*, 2002]. It is difficult to distinguish between these two effects because solar luminosity and GCR change coevally. However, long-term changes in GCR over the Phanerozoic are not related to changes in solar activity but are caused by the passage of the solar system through the spiral arms of our galaxy. Hence the Phanerozoic GCR-climate correlation is clearly not caused by changes in solar luminosity suggesting that Holocene climate might also be influenced by GCR rather than solar luminosity.

[61] The model presented in this paper confirms that an increase in GCR flux by 1% would induce an increase in average global surface temperature of about 0.14°C at a constant pCO_2 level. On long geological timescales pCO_2 compensates for GCR-induced climate change due to the negative weathering feedback. However, on

Table A1. Carbon and Sr Fluxes (in 10^{+18} mol/Myr) and Related Variables Considered in the Model

Flux	Equation
CO_2 release via mantle degassing	$F_M = f_{VO} \cdot F_M\,(Q)$
$CaCO_3$ formation during alteration of oceanic crust	$F_{ALT} = \frac{CO(Q)}{CO} \cdot (r_{ALT} \cdot (f_{VO} - 1) + 1) \cdot F_{ALT}(Q)$
CO_2/HCO_3 turnover due to silicate weathering	$F_{WS} = f(CO_2) \cdot f(T) \cdot (f_A \cdot f_D)^{0.65} \cdot f_E \cdot (f_{ER}^{eWB} \cdot f_{VO} \cdot F_{WS}^{VO}(Q) + f_{ER}^{eWS} \cdot F_{WS}^{S}(Q))$
CO_2 consumption due to carbonate weathering	$F_{WC} = f(CO_2) \cdot f_C\,(T) \cdot f_{ER}^{eWC} \cdot f_{LA} \cdot f_D \cdot f_E \cdot k_{WC} \cdot CC$
Effect of CO_2 on weathering[a]	$f(CO_2) = \frac{1}{1 + e^{\frac{t+365}{5}}} \cdot RCO_2^{0.5} + \left(1 - \frac{1}{1 + e^{\frac{t+365}{5}}}\right) \cdot \left(\frac{2 \cdot RCO_2}{1 + RCO_2}\right)^{0.4}$
Effect of temperature on silicate weathering	$f(T) = e^{ACT \cdot (T - T(Q))} \cdot (1 + RUN \cdot (T - T(Q)))^{0.65}$
Effect of temperature on carbonate weathering	$f_C(T) = 1 + 0.087 \cdot (T - T(Q))$
CO_2 release due to metamorphism of continental carbonates	$F_{MC} = k_{MC} \cdot CC$
CO_2 release due to carbonate burial	$F_{BC} = k_{BC} \cdot \left(\frac{Ca \cdot CO_3}{k_{SP}} - 1\right)$
Burial of pelagic carbonates	$F_{BCO} = (1 - f_{BCC}) \cdot F_{BC}$
Burial of carbonates on continental crust	$F_{BCC} = f_{BCC} \cdot F_{BC}$
CO_2 release at subduction zones from subducted $CaCO_3$	$F_{SC} = r_S \cdot f_{VO} \cdot k_{SC} \cdot CO$
$CaCO_3$ subduction into the mantle	$F_{SM} = (1 - r_S) \cdot f_{VO} \cdot k_{SC} \cdot CO$
CO_2 release due to weathering and metamorphism of POC	$F_{WO} = f_{ER}^{eWS} \cdot f_A \cdot F_{WO}(Q)$
CO_2 uptake due to POC accumulation	$F_{BO} = k_{BO} \cdot (\delta^{13}C_{DAT} - \delta^{13}C_{MOD})$
CO_2 exchange between ocean and atmosphere	$F_{EX} = k_{EX} \cdot (pCO_2^{SW} - pCO_2^{ATM})$
Hydrothermal Sr release	$F_{HY}^{Sr} = f_{VO} \cdot F_{HY}^{Sr}(Q)$
Sr release due to silicate weathering	$F_{WS}^{Sr} = f(CO_2) \cdot f(T) \cdot (f_A \cdot f_D)^{0.65} \cdot f_E \cdot (f_{ER}^{eWB} \cdot f_{VO} \cdot F_{WS,Sr}^{VO}\,(Q) + f_{ER}^{eWS} \cdot F_{WS,Sr}^{S}(Q))$
Sr release due to carbonate weathering	$F_{WC}^{Sr} = r_{SrC} \cdot F_{WC}$
Sr removal from the ocean	$F_B^{Sr} = k_{BSr} \cdot \left(\frac{C_{Sr}}{C_{Ca}} - (Sr/Ca)_{DAT}\right)$
^{87}Sr release due to silicate weathering	$F_{WS}^{87} = f(CO_2) \cdot f(T) \cdot (f_A \cdot f_D)^{0.65} \cdot f_E \cdot (f_{ER}^{eWB} \cdot f_{VO} \cdot \Phi_{87}^{VO} \cdot F_{WS,Sr}^{VO}\,(Q) + f_{ER}^{eWS} \cdot \Phi_{87}^{S} \cdot F_{WS,Sr}^{S}\,(Q))$

[a] The exponential Boltzmann terms are introduced to force a continuous change in weathering rate law over the time period of 380–350 Ma when land plants appeared and spread over the continents [*Berner and Kothavala*, 2001]. The model time t used in the exponential terms runs from −560 Ma to 0 Ma.

shorter timescales the pCO_2 value is not controlled by rates of silicate weathering so that external cooling is not accompanied by an increase in pCO_2. Thus the glacial/interglacial cycles of the late Quaternary climate are amplified rather than dampened by coeval pCO_2 changes [*Petit et al.*, 1999] and the global cooling during the early 90s of the 20th century induced by the Pinatubo volcanic explosion was accompanied by a drop in pCO_2 presumably related to diminished respiration rates [*Jones and Cox*, 2001]. Svensmark's hypothesis that short-term variations in GCR induced by solar activity change contribute significantly to natural climate variability is confirmed by the new results presented in this paper. This does not imply that future climate change will be dominated by changes in solar activity because the strong anthropogenic pCO_2 increase projected by IPCC will probably have a much larger climate effect [*Intergovernmental Panel on Climate Change* (*IPCC*), 2001]. It seems that the history of 20th century climate change was strongly related to natural GCR variability while the secular climate change of the new century will be dominated by man-made greenhouse gas effects.

Appendix A

[62] Carbon and Sr fluxes (in 10^{+18} mol/Myr) and related variables considered in the model are given in Table A1. Parameter values used in the definition of carbon and Sr fluxes are given in Table A2. Water fluxes and ^{18}O turnover considered in the model are given in Table A3. Parameter values used in the definition of water and ^{18}O fluxes are

Table A2. Parameter Values Used in the Definition of Carbon and Sr Fluxes[a]

Parameter	Symbol/Value
Quaternary CO_2 release via mantle degassing (10^{18} mol Ma^{-1})	$F_M(Q) = 1.5$
Quaternary CO_2 consumption via weathering of basaltic rocks (10^{18} mol Ma^{-1})	$F_{WS}{}^{VO}(Q) = 3 \times 0.5^{eWB}$
Quaternary CO_2 consumption via weathering of other silicate rocks (10^{18} mol Ma^{-1})	$F_{WS}{}^{S}(Q) = 8.7 \times 0.5^{eWS}$
Quaternary CO_2 release via weathering and metamorphism of POC (10^{18} mol Ma^{-1})	$F_{WO}(Q) = 6$
Quaternary rate of $CaCO_3$ formation during oceanic crust alteration (10^{18} mol Ma^{-1})	$F_{ALT}(Q) = 1.5$
Quaternary Sr release via hydrothermal circulation (10^{15} mol Ma^{-1})	$F_{HY}{}^{Sr}(Q) = 3.9$
Quaternary Sr release via weathering of basaltic rocks (10^{15} mol Ma^{-1})	$F_{WS,Sr}{}^{VO}(Q) = 2.5 \times F_{WS}{}^{VO}(Q)$
Quaternary Sr release via weathering of other silicate rocks (10^{15} mol Ma^{-1})	$F_{WS,Sr}{}^{S}(Q) = 1.5 \times F_{WS}{}^{S}(Q)$
Kinetic constant for carbonate weathering (Ma^{-1})	$k_{WC} = 13 \times 0.5^{eWC}/4000$
Kinetic constant for carbonate accumulation (10^{18} mol Ma^{-1})	$k_{BC} = 100$
Kinetic constant for POC burial (10^{18} mol Ma^{-1})	$k_{BO} = 100$
Kinetic constant for the CO_2 sea - air flux (10^{18} mol atm^{-1} Ma^{-1})	$k_{EX} = 10^5$
Kinetic constant for metamorphism of continental carbonates (10^{-3} Ma^{-1})	$k_{MC} = 0.55$
Kinetic constant for the subduction of oceanic plates (Ma^{-1})	$k_{SC} = 0.01$
Kinetic constant for volcanic/tectonic activity	$k_V = 10^5$
Kinetic constant for Sr removal from seawater (10^{18} mol Ma^{-1})	$k_{BSr} = 100$
Effect of erosion on silicate weathering	eWS = 0.5
Effect of erosion on basalt weathering	eWB = 0.2
Effect of erosion on carbonate weathering	eWC = 0.2
Fraction of subducted $CaCO_3$ degassing into the atmosphere	$r_S = 0.3$
Fraction of authigenic $CaCO_3$ formation occurring close to spreading centers	$r_{ALT} = 1.0$
Ratio between Sr release and CO_2 consumption during carbonate weathering	$r_{SrC} = 6.25 \times 10^{-4}$
Activation energy for silicate weathering ($°C^{-1}$)	ACT = 0.09
Impact of solar luminosity on surface temperature (°C)	$w_S = 7.4$
Mole fraction of ^{13}C in mantle CO_2	$\Phi_M = 0.01106$
Mole fraction of ^{13}C in weathering carbonate rocks	$\Phi_C = 0.01113$
Mole fraction of ^{13}C in weathering POC	$\Phi_O = 0.0108101$
Mole fraction of ^{13}C in buried carbonate sediments	$\Phi_{TC} = {}^{13}C/TC$
Mole fraction of ^{13}C in buried POC	$\Phi_{POC} = \frac{\alpha_{POC} \cdot \Phi_{TC}}{\alpha_{POC} \cdot \Phi_{TC} + 1 - \alpha_{POC}}$
Mole fraction of ^{87}Sr in weathering basaltic rocks	$\Phi_{87}{}^{VO} = 0.0695609$
Mole fraction of ^{87}Sr in other weathering silicate rocks	$\Phi_{87}{}^{S} = 0.0705697$
Mole fraction of ^{87}Sr in weathering carbonate rocks	$\Phi_{87}{}^{C} = 0.0698363$
Mole fraction of ^{87}Sr in hydrothermal fluids	$\Phi_{87}{}^{HY} = 0.0693314$
Mole fraction of ^{87}Sr in seawater	$\Phi_{87}{}^{SW} = {}^{87}Sr/Sr$

[a] Values were taken from *Wallmann* [2001a; 2001b], *Hansen and Wallmann* [2003], and further sources discussed in the text.

Table A3. Water Fluxes and ^{18}O Turnover Considered in the Model

Flux	Equation
H_2O fixation in weathering products	$F_{WSH} = r_{WS} \cdot F_{WS}$
H_2O uptake in upper crust (0–500 m)	$F_{ALTH} = r_{ALTH} \cdot F_{ALT}$
H_2O uptake in deep crust (>0.5 km)	$F_{SP} = f_{VO} \cdot F_{SP}(Q)$
H_2O uptake in serpentinite	$F_{SER} = F_{SER}(Q)$
H_2O uptake in continental ice shields	$F_{FR} = A \cdot \left(e^{\frac{(t-tg)^2}{2 \cdot w^2}} + e^{-\frac{t^2}{w^2}} \right)$
H_2O release from weathering products	$F_{REW} = k_{ME} \cdot CLAY$
H_2O release from upper crust and serpentinite at subduction zones	$F_{REUP} = r_{UP} \cdot k_S \cdot f_{VO} \cdot UP$
H_2O release from deep crust and serpentinite at subduction zones	$F_{REDEEP} = r_{DEEP} \cdot k_S \cdot f_{VO} \cdot DEEP$
Subduction of upper crustal H_2O into the mantle	$F_{SUP} = (1 - r_{UP}) \cdot k_S \cdot f_{VO} \cdot UP$
Subduction of deep crustal H_2O into the mantle	$F_{SDEEP} = (1 - r_{DEEP}) \cdot k_S \cdot f_{VO} \cdot DEEP$
H_2O release through mantle degassing	$F_{MH} = r_V \cdot F_M$
H_2O release via ice melting	$F_{MEL} = A \cdot \left(e^{-\frac{(t-tg-w)^2}{2 \cdot w^2}} \right)$
Uptake of mantle H_2O in upper crust at spreading centers	$F_{MUH} = f_{VO} \cdot F_{MUH}(Q)$
Uptake of mantle H_2O in deep crust at spreading centers	$F_{MDH} = f_{VO} \cdot F_{MDH}(Q)$
Isotopic exchange during alteration of upper crust at low temperatures	$F_{EX}^{UP} = (\Phi_{BAS} - \Phi_{ALT}^{i}) \cdot r_{ALTO} \cdot F_{ALT}$
Isotopic exchange during alteration of deep crust at high temperatures	$F_{EX}^{DEEP} = (\Phi_{BAS} - \Phi_{SP}^{i}) \cdot r_{SPO} \cdot F_{SP}$
Isotopic exchange during weathering of silicate rocks	$F_{EX}^{WS} = (\Phi_{SI} - \Phi_{WS}^{i}) \cdot r_{WSO} \cdot F_{WS}$
Mole fraction of ^{18}O in instantaneous products of low-temperature alteration of upper oceanic crust	$\Phi_{ALT}^{i} = \frac{\alpha_{ALT} \cdot \Phi_{SW}}{\alpha_{ALT} \cdot \Phi_{SW} + 1 - \Phi_{SW}}$
Mole fraction of ^{18}O in instantaneous products of high-temperature alteration of deep oceanic crust	$\Phi_{SP}^{i} = \frac{\alpha_{SP} \cdot \Phi_{SW}}{\alpha_{SP} \cdot \Phi_{SW} + 1 - \Phi_{SW}}$
Mole fraction of ^{18}O in instantaneous products of silicate weathering	$\Phi_{WS}^{i} = \frac{\alpha_{WS} \cdot \Phi_{SW}}{\alpha_{WS} \cdot \Phi_{SW} + 1 - \Phi_{SW}}$
Mole fraction of ^{18}O in instantaneously formed ice	$\Phi_{FR}^{i} = \frac{\alpha_{FR} \cdot \Phi_{SW}}{\alpha_{FR} \cdot \Phi_{SW} + 1 - \Phi_{SW}}$
Mole fraction of ^{18}O in continental ice shields	$\Phi_{ICE} = \frac{^{18}ICE}{ICE}$

Table A4. Parameter Values Used in the Definition of Water and ^{18}O Fluxes[a]

Parameter	Symbol/Value
Ratio of H_2O uptake and CO_2 consumption during silicate weathering	$r_{WS} = 1$
Ratio of H_2O uptake and $CaCO_3$ formation during alteration of upper crust	$r_{ALTH} = 3$
Ratio between H_2O and CO_2 release during mantle degassing	$r_V = 1$
Ratio of O turnover and $CaCO_3$ formation during alteration of upper crust	$r_{ALTO} = 15$
Ratio of O turnover and CO_2 consumption during silicate weathering	$r_{WSO} = 10$
Ratio of O turnover and H_2O uptake during alteration of deep crust	$r_{SPO} = 20$
Quaternary rate of H_2O fixation during alteration of deep crust	$F_{SP}(Q) = 10 \times 10^{+18}$ mol Ma^{-1}
Quaternary rate of H_2O fixation in serpentinite	$F_{SER}(Q) = 20 \times 10^{+18}$ mol Ma^{-1}
Quaternary uptake of mantle H_2O in upper crust at spreading centers	$F_{MUH}(Q) = 0.5 \times 10^{+18}$ mol Ma^{-1}
Quaternary uptake of mantle H_2O in deep crust at spreading centers	$F_{MDH}(Q) = 5.5 \times 10^{+18}$ mol Ma^{-1}
Kinetic constant for the metamorphic release of H_2O from sedimentary rocks	$k_{ME} = 1 \times 10^{-3}$ Ma^{-1}
Kinetic constant defining the subduction of oceanic crust	$k_S = 0.01$ Ma^{-1}
Fraction of H_2O in subducted upper crust recycled into the atmosphere	$r_{UP} = 0.9$
Fraction of H_2O in subducted deep crust recycled into the atmosphere	$r_{DEEP} = 0.6$
Fraction of serpentinization occurring at low temperatures in shallow crust	$r_{SER} = 0.3$
Amplitude of freezing and melting fluxes	$A = 122 \times 10^{+18}$ mol Ma^{-1}
Width of freezing and melting periods	$w = 25$ Ma
Time of maximum glaciation	$t_g = 270$ Ma
Isotopic fractionation factor for O turnover during silicate weathering	$\alpha_{WS} = 1.02$
Isotopic fractionation factor for O turnover during alteration of upper crust at low temperatures	$\alpha_{ALT} = 1.015$
Isotopic fractionation factor for O turnover during alteration of deep crust at high temperatures	$\alpha_{SP} = 1$
Isotopic fractionation factor for the formation of continental ice shields	$\alpha_{FR} = 0.96$
^{18}O mole fraction in weathering silicate rocks	$\Phi_{SI} = 2.017 \times 10^{-3}$
^{18}O mole fraction in fresh oceanic crust	$\Phi_{BAS} = 2.0126 \times 10^{-3}$
^{18}O mole fraction in mantle water	$\Phi_M = 2.015 \times 10^{-3}$
^{18}O mole fraction in water released from upper crust at arc volcanoes	$\Phi_{SU} = 2.021 \times 10^{-3}$
^{18}O mole fraction in water released from deep crust at arc volcanoes	$\Phi_{SD} = 2.015 \times 10^{-3}$
^{18}O mole fraction in water released during metamorphism of sedimentary rocks	$\Phi_{MS} = 2.021 \times 10^{-3}$

[a] Values were taken from *Wallmann* [2001a; 2001b].

Table A5. Mass Balances Considered in the Box Model[a]

Reservoir	Differential Equation
CO_2 in the atmosphere	$\frac{dCO_2}{dt} = + F_{EX}$
Total dissolved inorganic carbon in the ocean	$\frac{dTC}{dt} = F_M + F_{MC} + F_{SC} + F_{WC} + F_{WO} - F_{BC} - F_{BO} - F_{ALT} - F_{EX}$
Carbonate alkalinity in the ocean	$\frac{dCA}{dt} = +F_{WS} + 2 \cdot F_{WC} - 2 \cdot F_{BC} - F_{ALT}$
$CaCO_3$ deposited on and in oceanic crust	$\frac{dCO}{dt} = +F_{BCO} + F_{ALT} - F_{SC} - F_{SM}$
$CaCO_3$ deposited on continental crust	$\frac{dCC}{dt} = +F_{BCC} - F_{WC} - F_{MC}$
Total dissolved inorganic ^{13}C in the ocean	$\frac{d^{13}C}{dt} = \Phi_M \cdot F_M + \Phi_C \cdot (F_{MC} + F_{SC} + F_{WC}) + \Phi_O \cdot F_{WO} - \Phi_{TC} \cdot (F_{BC} - F_{ALT} - F_{EX}) - \Phi_{POC} \cdot F_{BO}$
Sr in the ocean	$\frac{dSr}{dt} = +F_{WS}^{Sr} + F_{WC}^{Sr} + F_{HY}^{Sr} - F_B^{Sr}$
^{87}Sr in the ocean	$\frac{d^{87}Sr}{dt} = +F_{WS}^{87} + \Phi_{87}^{C} \cdot F_{WC}^{Sr} + \Phi_{87}^{HY} \cdot F_{HY}^{Sr} - \Phi_{87}^{SW} \cdot F_B^{Sr}$
H_2O in the ocean	$\frac{dH_2O}{dt} = F_{REW} + F_{REUP} + F_{REDEEP} + F_{MH} + F_{MEL} - F_{WSH} - F_{ALTH} - F_{SP} - F_{SER} - F_{FR}$
H_2O in upper crust	$\frac{dUP}{dt} = F_{ALTH} + F_{MUH} + r_{SER} \cdot F_{SER} - F_{REUP} - F_{SUP}$
H_2O in deep crust	$\frac{dDEEP}{dt} = F_{SP} + F_{MDH} + (1 - r_{SER}) \cdot F_{SER} - F_{REDEEP} - F_{SDEEP}$
H_2O in sedimentary rocks	$\frac{dCLAY}{dt} = F_{WSH} - F_{REW}$
H_2O in continental ice	$\frac{dICE}{dt} = F_{FR} - F_{MEL}$
H_2O in the earth's mantle	$\frac{dMANTLE}{dt} = F_{SUP} + F_{SDEEP} - F_{MH} - F_{MUH} - F_{MDH}$
Change in free $H_2{}^{18}O$ mass	$\frac{dH_2{}^{18}O}{dt} = F_{EX}^{UP} + F_{EX}^{DEEP} + F_{EX}^{WS} + \Phi_{MS} \cdot F_{REW} + \Phi_{SU} \cdot F_{REUP} + \Phi_{SD} \cdot F_{REDEEP} + \Phi_M \cdot F_{MH} + \Phi_{ICE} \cdot F_{MEL} - \Phi_{WS}^{i} \cdot F_{WSH} - \Phi_{ALT}^{i} \cdot F_{ALTH} - \Phi_{SP}^{i} \cdot F_{SP} - \Phi_{ALT}^{i} \cdot r_{SER} \cdot F_{SER} - \Phi_{SP}^{i} \cdot (1 - r_{SER}) \cdot F_{SER} - \Phi_{FR}^{i} \cdot F_{FR}$
$H_2{}^{18}O$ in continental ice	$\frac{d^{18}ICE}{dt} = \Phi_{FR}^{i} \cdot F_{FR} - \Phi_{ICE} \cdot F_{MEL}$

[a] In 10^{+18} mol.

given in Table A4. Mass balances considered in the Box Model are given in Table A5.

Acknowledgments

[63] The work was supported by the DFG within the SFB 574 "Volatiles and Fluids in Subduction Zones" located at Kiel University. This paper is contribution 61 of SFB 574. The author would like to thank Bob Berner, Jan Veizer, and Thomas Mentel for stimulating discussions and helpful comments.

References

Abbott, D. H., and A. E. Isley (2002), The intensity, occurrence, and duration of superplume events and eras over geological time, *J. Geodyn.*, *34*, 265–307.

Alt, J. C. (2003), Stable isotopic composition of upper oceanic crust formed at a fast spreading ridge, ODP Site 801, *Geochem. Geophys. Geosyst.*, *4*(5), 8908, doi:10.1029/2002GC000400.

Archer, D. E. (1996), An atlas of the distribution of calcium carbonate in sediments of the deep sea, *Global Biogeochem. Cycles*, *10*(1), 159–174.

Barron, E. J., P. J. Fawcett, W. H. Peterson, D. Pollard, and S. L. Thompson (1995), A "simulation" of mid-Cretaceous climate, *Paleoceanography*, *10*(5), 953–962.

Berner, R. A. (1991a), Atmospheric carbon dioxide levels over Phanerozoic time, *Science*, *249*, 1382–1386.

Berner, R. A. (1991b), A model for atmospheric CO_2 over Phanerozoic time, *Am. J. Sci.*, *291*, 339–376.

Berner, R. A. (1992), Weathering, plants, and the long-term carbon cycle, *Geochim. Cosmochim. Acta*, *56*, 3225–3231.

Berner, R. A. (1994), GEOCARB II: A revised model of atmospheric CO_2 over Phanerozoic time, *Am. J. Sci.*, *294*, 56–91.

Berner, R. A. (1997), The rise of plants and their effect on weathering and atmospheric CO_2, *Science*, *276*, 544–546.

Berner, R. A., and Z. Kothavala (2001), GEOCARB III: A revised model of atmospheric CO_2 over Phanerozoic time, *Am. J. Sci.*, *301*, 182–204.

Berner, R. A., A. C. Lasaga, and R. M. Garrels (1983), The carbonate-silicate geochemical cycle and its effect on atmo-

spheric carbon dioxide over the past 100 million years, *Am. J. Sci.*, *283*, 641–683.

Bluth, G. J. S., and L. R. Kump (1991), Phanerozoic paleogeology, *Am. J. Sci.*, *291*, 284–308.

Bond, G., B. Kromer, J. Beer, R. Muscheler, M. N. Evans, W. Showers, S. Hoffmann, R. Lotti-Bond, I. Hajdas, and G. Bonani (2001), Persistent solar influence on North Atlantic Climate during the Holocene, *Science*, *294*, 2130–2136.

Boucot, A. J., and J. Gray (2001), A critique of Phanerozoic climatic models involving changes in the CO_2 content of the atmosphere, *Earth Sci. Rev.*, *56*, 1–159.

Brand, U., A. Logan, N. Hiller, and J. Richardson (2003), Geochemistry of modern brachiopods: Applications and implications for oceanography and paleoceanography, *Chem. Geol.*, *198*, 305–334.

Broecker, W. S., and T.-H. Peng (1982), *Tracers in the Sea*, 690 pp., Lamont-Doherty Geol. Obs., Columbia Univ., Palisades, N. Y.

Charlou, J. L., J. P. Donval, Y. Fouquet, P. Jean-Baptiste, and N. Holm (2002), Geochemistry of high H_2 and CH_4 vent fluids issuing from ultramafic rocks at the Rainbow hydrothermal field (36°14′N, MAR), *Chem. Geol.*, *191*, 345–359.

Crowley, T. J., and R. A. Berner (2001), CO_2 and climate change, *Science*, *292*, 870–872.

Davis, A. C., M. J. Bickle, and D. A. H. Teagle (2003), Imbalance in the oceanic strontium budget, *Earth Planet. Sci. Lett.*, *211*, 173–187.

Fischer, A. G. (1981), Climatic oscillations in the biosphere, in *Biotic Crisis in Ecological and Evolutionary Time*, edited by M. H. Nitecki, pp. 103–131, Academic, San Diego, Calif.

Fisher, A. T., and K. Becker (2000), Channelized fluid flow in oceanic crust reconciles heat-flow and permeability data, *Nature*, *403*, 71–74.

Foukal, P. (2002), A comparison of variable swolar total and ultraviolet irradiance outputs in the 20th century, *Geophys. Res. Lett.*, *29*(23), 2089, doi:10.1029/2002GL015474.

Frakes, L. A., J. E. Francis, and J. I. Syktus (1992), *Climate Modes of the Phanerozoic*, 274 pp., Cambridge Univ. Press, New York.

Gibbs, M. T., G. J. S. Bluth, P. J. Fawcett, and L. R. Kump (1999), Global chemical erosion over the last 250 My: Variations due to changes in paleogeography, paleoclimate, and paleogeology, *Am. J. Sci.*, *299*, 611–651.

Gradstein, F. M., F. P. Agterberg, J. G. Ogg, J. Hardenbol, P. v. Veen, J. Thierry, and Z. Huang (1995), A Triassic, Jurassic and Cretaceous time scale, in *Geochronology, Time Scales, and Global Stratigraphic Correlation*, edited by W. A. Bergrgen et al., pp. 95–126, Soc. Sediment. Geol. (SEPM), Tulsa, Okla.

Gregor, C. B. (1985), The mass-age distribution of Phanerozoic sediments, in *The Chronology of the Geological Record*, edited by N. J. Snelling, pp. 284–288, Blackwell Sci., Malden, Mass.

Hallam, A. (1992), *Phanerozoic Sea-Level Changes*, 266 pp., Columbia Univ. Press, New York.

Hansen, K. W., and K. Wallmann (2003), Cretaceous and Cenozoic evolution of seawater composition, atmospheric O_2 and CO_2: A model perspective, *Am. J. Sci.*, *303*, 94–148.

Harland, W. B., R. L. Armstrong, A. V. Cox, L. E. Craig, A. G. Smith, and D. G. Smith (1990), *A Geologic Time Scale*, 263 pp., Cambridge Univ. Press, New York.

Hay, W. W. (1998), Carbonate sedimentation through the late Precambrian and Phanerozoic, *Zbl. Geol. Paläont. Teil I*, *1998*(5–6), 435–445.

Hayes, J. M., H. Strauss, and A. J. Kaufman (1999), The abundance of ^{13}C in marine organic matter and isotopic fractionation in the global biogeochemical cycle of carbon during the past 800 Ma, *Chem. Geol.*, *161*, 103–125.

Horita, J., H. Zimmermann, and H. D. Holland (2002), The chemical evolution of seawater during the Phanerozoic: Implications from the record of marine evaporites, *Geochim. Cosmochim. Acta*, *66*(21), 3733–3756.

Hu, F. S., D. Kaufman, S. Yoneji, D. Nelson, A. Shemesh, Y. Huang, J. Tian, G. Bond, B. Clegg, and T. Brown (2003), Cyclic variation and solar forcing of Holocene climate in the Alaskan subarctic, *Science*, *301*, 1890–1893.

Intergovernmental Panel on Climate Change (IPCC) (2001), *Climate Change 2001: Synthesis Report. A Contribution of Working Groups I, II, and III to the Third Assessment Report of the Intergovernmental Panel on Climate Change*, 398 pp., Cambridge Univ. Press, New York.

Jacobson, A. D., J. D. Blum, and L. M. Walter (2002), Reconciling the elemental and Sr isotope composition of Himalayan weathering fluxes: Insights from the carbonate geochemistry of stream waters, *Geochim. Cosmochim. Acta*, *66*(19), 3417–3429.

Jacobson, A. D., J. D. Blum, C. P. Chamberlain, D. Craw, and P. O. Koons (2003), Climatic and tectonic controls on chemical weathering in the New Zealand Southern Alps, *Geochim. Cosmochim. Acta*, *67*(1), 29–46.

Jones, C. D., and P. M. Cox (2001), Modeling the volcanic signal in the atmospheric CO_2 record, *Global Biogeochem. Cycles*, *15*(2), 453–465.

Kim, S.-T., and J. R. O'Neil (1997), Equilibrium and nonequilibrium oxygen isotope effects in synthetic carbonates, *Geochim. Cosmochim. Acta*, *61*(16), 3461–3475.

Kniveton, D. R., and M. C. Todd (2001), On the relationship of cosmic ray flux and precipitation, *Geophys. Res. Lett.*, *28*(8), 1527–1530.

Kothavala, Z., R. J. Oglesby, and B. Saltzman (1999), Sensitivity of equilibrium surface temperature of CCM3 to systematic changes in atmospheric CO_2, *Geophys. Res. Lett.*, *26*(2), 209–212.

Kothavala, Z., R. A. Berner, R. J. Oglesby, and B. Saltzman (2000a), Effect of paleogeography on paleoclimates with systematic increases in atmospheric CO_2, *Trans. AGU*, *81*(48), Fall Meet. Suppl., Abstract OS22H-12.

Kothavala, Z., R. J. Oglesby, and B. Saltzman (2000b), Evaluating the climatic response to changes in CO_2 and solar luminosity, paper presented at 11th Symposium on Global Change Studies, Am. Meteorol. Soc., Long Beach, Calif.

Lear, C. H., H. Elderfield, and P. A. Wilson (2000), Cenozoic deep-sea temperatures and global ice volumes from Mg/Ca in benthic foraminiferal calcite, *Science*, *287*, 269–272.

Lear, C. H., H. Elderfield, and P. A. Wilson (2003), A Cenozoic seawater Sr/Ca record from benthic foraminiferal

calcite and its application in determining global weathering fluxes, *Earth Planet. Sci. Lett.*, *208*, 69–84.

Mackenzie, F. T., L. M. Ver, and A. Lerman (2002), Century-scale nitrogen and phosphorus controls of the carbon cycle, *Chem. Geol.*, *190*, 13–32.

Maier-Reimer, E. (1993), Geochemical cycles in an ocean general circulation model, Preindustrial tracer distribution, *Global Biogeochem. Cycles*, *7*(3), 645–677.

Marsh, N., and H. Svensmark (2000a), Cosmic rays, clouds, and climate, *Space Sci. Rev.*, *94*, 215–231.

Marsh, N., and H. Svensmark (2000b), Low cloud properties influenced by cosmic rays, *Phys. Rev. Lett.*, *85*, 5004–5007.

Millero, F. J. (1996), *Chemical Oceanography*, 469 pp., CRC Press, Boca Raton, Fla.

Neff, U., S. J. Burns, A. Mangini, M. Mudelsee, D. Fleitmann, and A. Matter (2001), Strong coherence between solar variability and the monsoon in Oman between 9 and 6 kyr ago, *Nature*, *411*, 290–293.

Niggemann, S., A. Mangini, M. Mudelsee, D. K. Richter, and G. Wurth (2003), Sub-Milankovitch climatic cycles in Holocene stalagmites from Sauerland, Germany, *Earth Planet. Sci. Lett.*, *216*, 539–547.

Otto-Bliesner, B. L. (1995), Continental drift, runoff, and weathering feedbacks: Implications from climate model experiments, *J. Geophys. Res.*, *100*(D6), 1537–1548.

Petit, L. R., et al. (1999), Climate and atmospheric history of the past 42,0000 years from the Vostok ice core, Antarctica, *Nature*, *399*, 429–436.

Podlaha, O. G., J. Mutterlose, and J. Veizer (1998), Preservation of $\delta^{18}O$ and $\delta^{13}C$ in belemnite rostra from the Jurrasic/Early Cretaceous successions, *Am. J. Sci.*, *298*, 324–347.

Ronov, A. B. (1993), *Stratisfera - Ili Osadochnaya Obolochka Zemli* (*Kolichestvennoe Issledovanie*), edited by A. A. Yaroshevskii, Nauka, Moscow.

Royer, D. L., R. A. Berner, and D. J. Beerling (2001), Phanerozoic atmospheric CO_2 change: Evaluating geochemical and paleobiological approaches, *Earth Sci. Rev.*, *54*, 349–392.

Saal, A. E., E. H. Hauri, C. H. Langmuir, and M. R. Perfit (2002), Vapour undersaturatation in primitive mid-ocean-ridge basalt and the volatile content of Earth's upper mantle, *Nature*, *419*, 451–455.

Schmidt, M. W., and S. Poli (1998), Experimentally based water budgets for dehydrating slabs and consequences for arc magma generation, *Earth Planet. Sci. Lett.*, *163*, 361–379.

Shaviv, N. J. (2002a), Cosmic ray diffusion from the galactic spiral arms, iron meteorites, and a possible climatic connection, *Phys. Rev. Lett.*, *89*(5), 051,102.

Shaviv, N. J. (2002b), The spiral structure of the milky way, cosmic rays, and ice age epochs on earth, *New Astron.*, *8*, 39–77.

Shaviv, N. J., and J. Veizer (2003), Celestial driver of Phanerozoic climate?, *GSA Today*, *13*, 4–10.

Shields, G., and J. Veizer (2002), The Precambrian marine carbonate isotope database: Version 1.1, *Geochem. Geophys. Geosyst.*, *3*(6), 1031, doi:10.1029/2001GC000266.

Spero, H. J., J. Bijma, D. W. Lea, and B. E. Bemis (1997), Effect of seawater carbonate concentration on foraminiferal carbon and oxygen isotopes, *Nature*, *390*, 497–500.

Steuber, T., and J. Veizer (2002), Phanerozoic record of plate-tectonic control of seawater chemistry and carbonate sedimentation, *Geology*, *30*(12), 1123–1126.

Svensmark, H. (1998), Influence of cosmic rays on earth's climate, *Phys. Rev. Lett.*, *81*, 5027.

Svensmark, H., and E. Friis-Christensen (1997), Variation of cosmic ray flux and global cloud coverage - a missing link in solar-climate relationships, *J. Atmos. Sol. Terr. Phys.*, *59*(11), 1225–1232.

Tardy, Y., R. N'Kounkou, and J.-L. Probst (1989), The global water cycle and continental erosion during Phanerozoic time (570 my), *Am. J. Sci.*, *289*, 455–483.

Usdowski, E., and J. Hoefs (1993), Oxygen isotope exchange between carbonic acid, bicarbonate, carbonate, and water: A re-examination of the data of McCrea [1950] and an expression for the overall partitioning of oxygen isotopes between the carbonate species and water, *Geochim. Cosmochim. Acta*, *57*, 3815–3818.

Van Andel, T. J. H. (1975), Mesozoic/Cenozoic calcite compensation depth and the global distribution of calcareous sediments, *Earth Planet. Sci. Lett.*, *26*, 187–194.

Veizer, J., P. Bruckschen, F. Pawellek, A. Diener, O. G. Podlaha, G. A. F. Carden, T. Jasper, C. Korte, H. Strauss, K. Azmy, and D. Ala (1997), Oxygen isotope evolution of Phanerozoic seawater, *Palaeogeography, Palaeoclimatology, Palaeoecology*, *132*, 159–172.

Veizer, J., et al. (1999), $^{87}Sr/^{86}Sr$, $\delta^{13}C$, and $\delta^{18}O$ evolution of Phanerozoic seawater, *Chem. Geol.*, *161*, 59–88.

Veizer, J., Y.-F. Goddéris, and L. M. François (2000), Evidence for decoupling of atmospheric CO_2 and global climate during the Phanerozoic eon, *Nature*, *408*, 698–701.

Walker, J. C. G., P. B. Hays, and J. F. Kasting (1981), A negative feedback mechanism for the long-term stabilization of Earth's surface temperature, *J. Geophys. Res.*, *86*, 9776–9782.

Wallmann, K. (2001a), Controls on Cretaceous and Cenozoic evolution of seawater composition, atmospheric CO_2 and climate, *Geochim. Cosmochim. Acta*, *65*(18), 3005–3025.

Wallmann, K. (2001b), The geological water cycle and the evolution of marine $\delta^{18}O$ values, *Geochim. Cosmochim. Acta*, *65*(15), 2469–2485.

Yu, F. (2002), Altitude variations of cosmic ray induced production of aerosols: Implications for global cloudiness and climate, *J. Geophys. Res.*, *107*(A7), 1118, doi:10.1029/2001JA000248.

Zeebe, R. E. (1999), An explanation of the effect of seawater carbonate concentration on foraminiferal oxygen isotopes, *Geochim. Cosmochim. Acta*, *63*(13/14), 2001–2009.

Zeebe, R. E. (2001), Seawater pH and isotopic paleotemperatures of Cretaceous oceans, *Palaeogeogr. Palaeoclimatol. Palaeoecol.*, *170*, 49–57.

Zeebe, R., and D. Wolf-Gladrow (2001), *CO_2 in Seawater: Equilibrium, Kinetics and Isotopes*, 346 pp., Elsevier Sci., New York.